Tellus (2003), 55A, 275–300
Printed in UK. All rights reserved

TELLUS
ISSN 0280–6495

A new approach to the cumulus parameterization issue

By T. N. KRISHNAMURTI* and J. SANJAY¶, *Department of Meteorology, Florida State University, Tallahassee, FL 32306-4520, USA*

(Manuscript received 9 September 2002; in final from 11 February 2003)

ABSTRACT

Can the superensemble methodology provide improved precipitation forecasts by combining existing physical parameterizations? We recently addressed this question in the context of Numerical Weather Prediction (NWP). We feel, however, that the information provided here may be useful for seasonal climate modeling as well. In the NWP context, we have developed multi-model forecasts from six versions of the Florida State University global spectral model (at a horizontal resolution of 170 waves, triangular truncation). These different versions deployed six different cumulus parameterization schemes; these models were identical in all other aspects, including the initial states. Making the assumption that differences in short-range (one day) forecasts of precipitation arise largely from differences in the cumulus parameterization, a superensemble methodology, following a recent study, was deployed to assign geographically distributed weights to convective heating for the different cumulus parameterization schemes. This was done after completion of some 85 experiments for each model for the training phase of the superensemble. A new single spectral model was next designed that included the weighted sum of the six cumulus parameterization schemes strung out within this model. This model was next shown to outperform in NWP forecasts of precipitation compared to any of those models that used a single cumulus parameterization scheme. This merely suggests that no single, present scheme is superior to all other schemes over the entire tropical belt; they all seem to have some virtues over different geographical regions. This Unified collective scheme is physically based since it does carry mechanisms such as mass flux, moisture convergence, cloud detrainment, downdrafts, effects of sea surface temperature etc. that are explicitly carried within one or the other schemes. This collective scheme is, however, based on optimized weights for these processes that vary geographically. It is our premise that even if a new breakthrough in cumulus parameterization were to occur from the development of a new scheme, that scheme, at best, may only achieve a skill ranking of number three for precipitation forecasts. The first place, we noted, still belongs to a multi-model superensemble, based on the optimal combination of six separate models. The second place belongs to the single model that utilizes a strung out weighted sum of many cumulus parameterization schemes within it. The individual member models have larger precipitation forecast errors compared to the two above. The skills, here, are evaluated using standard metrics such as correlations, root mean square errors and the equitable threat scores; finally we also present the vertical profiles of the apparent heat source and the apparent moisture sink that also confirm these above findings.

1. Introduction

This present paper addresses precipitation forecasts from six versions of the FSU (a list of acronyms is presented in Table 1) global spectral model outlined in Appendix. The six versions deploy six different cumulus parameterization algorithms, these include three different versions of the Arakawa–Schubert scheme, a modified Kuo scheme, Kerry Emanuel scheme and Zhang and McFarlane scheme. This paper next addresses the precipitation forecasts for the FSU multi-model superensemble (Krishnamurti et al., 2001) that is developed from this array of models. It is followed

*Corresponding author.
e-mail: tnk@io.met.fsu.edu
¶Permanent affiliation: Indian Institute of Tropical Meteorology, Pune 411 008, India.

Table 1. *List of acronyms*

AMIP	Atmospheric Model Intercomparison Project
A-S	Arakawa–Schubert Cumulus Scheme
BMRC	Bureau of Meteorology Research Centre
CAPE	Convective Available Potential Energy
DMSP-SSM/I	Defense Meteorology Space Program-Special Sensor Microwave/Imager
ECMWF	European Centre for Medium range Weather Forecasts
ECS	Emanuel Cumulus Scheme
FSU	Florida State University
GPROF	Goddard Profiling (algorithm)
GSFC	Goddard Space Flight Center
JMA	Japan Meteorological Agency
NCAR	National Center for Atmospheric Research
NCEP	National Center for Environmental Prediction
NOGAPS	Navy Operational Global Atmospheric Prediction System
NRL	Naval Research Laboratory
NWP	Numerical Weather Prediction
RAS	Relaxed Arakawa–Schubert Cumulus Scheme
RPN	Recherche en Prévision Numérique
SAS	Simplified Arakawa–Schubert Cumulus Scheme
T170	170 wave Triangular truncation
TRMM	Tropical Rainfall Measuring Mission
TSDIS	TRMM Science Data and Information Service
UTC	Coordinated Universal Time
ZM	Zhang and McFarlane Cumulus Scheme

by the precipitation forecasts from a single Unified FSU global spectral model where a string of cumulus parameterization schemes are deployed within a single model. The relative weights for different cumulus parameterization schemes, within that single model, are based on multimodel superensemble forecasts of precipitation. These weights are determined from the performance of the individual models, each of which carries one cumulus parameterization scheme. Figure 1 provides a schematic outline of the modeling component of this paper. The top part identifies the forecasts from a single model that carries a single cumulus parameterization algorithm. The middle part shows our so-called "Unified model"; this is a single model that carries a string of cumulus parameterization schemes within it. The bottom part of the illustration conveys the forecasts from a multimodel superensemble, where each member model carries a single cumulus parameterization algorithm.

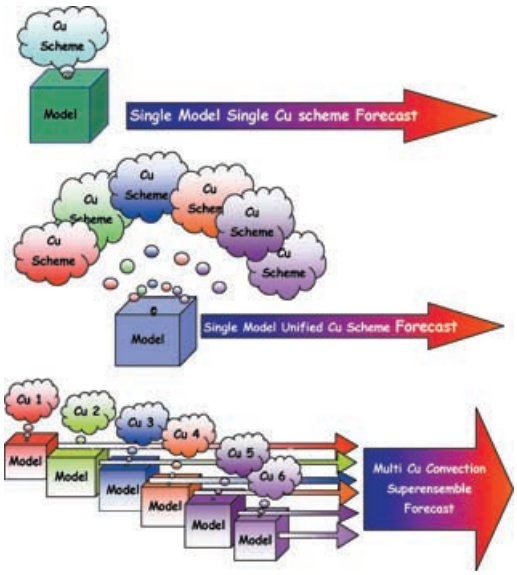

Fig. 1. A schematic outline of three types of models used in this study. (a) Single model running a single cumulus parameterization scheme. (b) A unified model (a single model) that carries all six cumulus parameterization schemes of this study. (c) A multimodel superensemble where each member model carries a single cumulus parameterization scheme.

Finally, this paper presents a comparison of the following precipitation forecasts: (a) performance of individual cumulus parameterization algorithms; (b) performance of Unified cumulus parameterization algorithms; and (c) performance of the FSU multimodel superensemble.

The purpose of this study is not to provide a detailed physical insight into the various cumulus parameterizations used here. We are merely examining the precipitation forecast capabilities of the member models, a Unified model and of the FSU superensemble. We also examine the heating and moistening profiles, along the vertical coordinate, in this same context.

The multimodels used in this study are derived from the FSU global spectral model at the resolution T170, see Appendix. In all 85 separate forecast experiments were first carried out using each of the six different versions of the cumulus parameterization. Thus, a total of 510 experiments were carried out to define what is called a training phase for a multimodel superensemble. The start dates for these experiments covered each of the days during the second week of April through June 2000 at 12 UTC. Details on these

experiments are presented in Shin and Krishnamurti (2003a,b).

The superensemble approach is a recent contribution to the general area of weather and climate forecasting, developed at the FSU, and is discussed in a series of publications by Krishnamurti et al. (1999, 2000a,b and 2001). The novelty of this approach lies in the methodology, which differs from ensemble analysis techniques used elsewhere. This approach yields forecasts with considerable reduction in forecast error compared to the error in the member models, the 'bias-removed' ensemble averaged forecast, and the ensemble mean. In brief, the technique entails the division of a time line into two parts. One part is a 'training' phase, where forecasts by a set of member models are compared to observed fields with the objective of developing a least squares fit of the forecasts to the observations. Specifically, the observed anomalies are fit to the member model forecasts according to the classical prescription

$$O' = \sum_{i=1}^{N} a_i (F_i - \overline{F}_i) + \varepsilon_i, \tag{1}$$

where F_i is the ith model forecast (out of N total models), $\overline{F}_i$ is the mean of the ith forecast over the training period, O' is the observed anomaly relative to the observed mean over the training period, the a_i values represent the regression coefficients and ε_i is an error term. The a_i are determined by requiring the summed squared error $E = \sum_{i=1}^{N} \varepsilon_i^2$ integrated over the training period to be as small as possible. A fit of this sort is performed for all model variables and at all model grid points for which reanalysis observations are available, and typically yields some 10^7 regression parameters. These may be thought of as bias correction weights. The second time line part is composed of genuine model predictions, i.e. the forecasts of the member models. The superensemble approach combines each of these forecasts according to the weights determined during the training period through the formulation

$$S = \bar{O} + \sum_{i=1}^{N} a_i (F_i - \overline{F}_i), \tag{2}$$

where the notation is defined above except the a_i values, which are the regression coefficients. The prediction S is referred to as the "superensemble" forecast. This forecast should be contrasted with the more standard anomaly forecasts known as the biased - removed ensemble mean (E) or ensemble mean ($\hat{E}$) forecasts:

$$E = \frac{1}{N} \sum_{i=1}^{N} (F_i - \overline{F}_i) \text{ or } \hat{E} = \frac{1}{N} \sum_{i=1}^{N} (F_i - \overline{O}). \tag{3}$$

The distinction between them comes in the weighting. Assigning all models a weight of unity in eq. (2) not only illustrates the connection between the forecasts, but also illustrates how the training period attempts to identify and highlight good model performance.

We have developed a real-time NWP capability for the forecast of all basic variables such as winds, temperature, surface pressure, geopotential heights and precipitation. These are multianalysis–multimodel superensemble forecasts where 11 models are used on a daily basis. These include the daily operational forecasts from the NCEP, Canadian Weather Service RPN, the Australian model for the BMRC, the U.S. Navy's NOGAPS, the Japanese model for JMA and different versions of the in-house FSU global spectral model physically initialized using different rain rate algorithms (see section 1.1). In one sense, the construction of the superensemble is a post-processing of multimodel forecasts. This is still a viable forecast product that is being prepared experimentally in real time at FSU and is currently available on a real-time basis on the website http://lexxy.met.fsu.edu/rtnwp. In medium range real-time global weather forecasts, the largest skill improvement is seen for precipitation forecasts both regionally and globally. The overall skill of the superensemble is 40–120% higher than the precipitation forecast skills of the best global models. For forecasts of variables other than precipitation, the superensemble exhibited major improvements in skill for the divergent part of the wind and the temperature distributions. Tropical latitudes show major improvements in daily weather forecasts. For most variables, we have used the operational ECMWF analysis at 0.5° latitude/longitude as the observed fields for the training phase.

Real-time hurricane track and intensity forecasts are another major component of superensemble modeling. This approach of carrying out a training phase followed by real-time forecasts has shown improved track and intensity predictions (up to 5 d) for the Atlantic hurricanes during 1999, 2000 and 2001. Improvements in track forecasts were 25–35% better than those of the participating member models. The intensity forecasts for hurricanes have been only marginally better than the best models. In some recent real-time tests during 1999, marked skill improvement in the forecasts of difficult storms such as Floyd and Lenny were noted where the performance of the superensemble

was considerably better than that of the member models.

The area of seasonal climate simulations has only been addressed recently in the context of atmospheric climate models where the sea surface temperatures and sea ice are prescribed, such as the AMIP data sets. In this context, given a training period of some 8 yr and a training data base from the ECMWF, the results exhibit improved skill compared to the member models and the ensemble mean. Preliminary work in this area (Krishnamurti et al., 2002) examines the difficulties involved with prediction of seasonal precipitation anomalies. Most individual member models perform poorly compared to climatology, whereas the superensemble appears to demonstrate precipitation skills slightly above those of climatology. The effectiveness of weather and seasonal climate forecasts from the superensemble methodology has also been assessed from measures of standard skill scores such as correlation against observed fields, root mean square (RMS) errors, anomaly correlations and the so-called Brier skill scores for climate forecasts (assessing skills above those of a climatology).

Training is a major component of this forecast initiative. We have compared training with the best quality 'observed' past data sets versus training deliberately with poorer data sets. This has shown that forecasts are improved when higher quality training data sets are deployed for the evaluation of the multimodel bias statistics. It was felt that the skill during the 'forecast phase' could be degraded if the training was executed with either a poorer analysis or poorer forecasts. This was noted in our recent work on precipitation forecasts, where we showed that the use of poorer rainfall estimates during the training period affected the superensemble forecasts during the 'forecast phase' (Krishnamurti et al., 2001). In addition, issues on optimizing the number of training days have been addressed from an examination of training with days of high forecast skill versus training with low forecast skill, and training with the best available rain-rate datasets versus those from poor representations of rain. We have learned to improve the forecast skill by selectively improving the distribution of weights during the training phase.

Why does the superensemble generally have higher skill compared to all participating multimodels and the ensemble mean? At each location and for all variables, the ensemble mean assigns a weight of $1/N$ to all N member models, including several poorer-performing models. As a result, assigning the same weight of $1/N$ to some poorer models was noted to degrade the skill of the ensemble mean. It is possible to remove the bias of models individually (at all locations and for all variables) and to perform an ensemble mean of the bias removed models. That, too, has somewhat lower skill compared to the superensemble, which carries selective weights distributed in space among all multimodels and for all variables. A poorer model does not reach the levels of the best models after its bias removal.

1.1. Summary of past work on precipitation superensemble

A major advance in precipitation forecasts has emerged from the use of a multimodel/multianalysis superensemble (Krishnamurti et al., 2001). "Multimodel" refers to different models whose forecasts are being assimilated for the construction of the superensemble. "Multianalysis" refers to different initial analyses contributing to forecasts from the same model. In this study, the multianalysis component is based on the FSU global spectral model initialized with TRMM and SSM/I data sets via a number of rain rate algorithms. Five different initial analyses for each day are deployed that define the multianalysis component. Those are based on different versions of rain rate estimates derived from TRMM and the DMSP-SSM/I satellites. The differences in the analyses arise from the use of these different rain rates within the physical initialization procedure outlined in Krishnamurti et al. (1991). The resulting initialized fields have distinct differences among their initial divergence, heating, moisture and rain rate descriptions. The five multimodel forecasts with diverse horizontal and vertical resolutions are received from a number of global operational centers. The model output is then interpolated to a common grid of the lowest resolution member model. Generally, the resulting horizontal resolution is around 125 km. The global models include several different parameterizations of physical processes; effects of ocean, snow and ice cover; and treatment of orography. The training data set is produced from the daily TSDIS operational files of the TRMM microwave radiometer-based rainfall estimates. In order to extend the global coverage, the observed data sets are augmented with the use of the SSM/I derived rain rates from the US Air Force polar orbiting DMSP satellites (F11, F13, F14 and F15).

Some recent skill scores are presented here from the 11-model multimodel/multianalysis superensemble, which includes other than the five multimodels

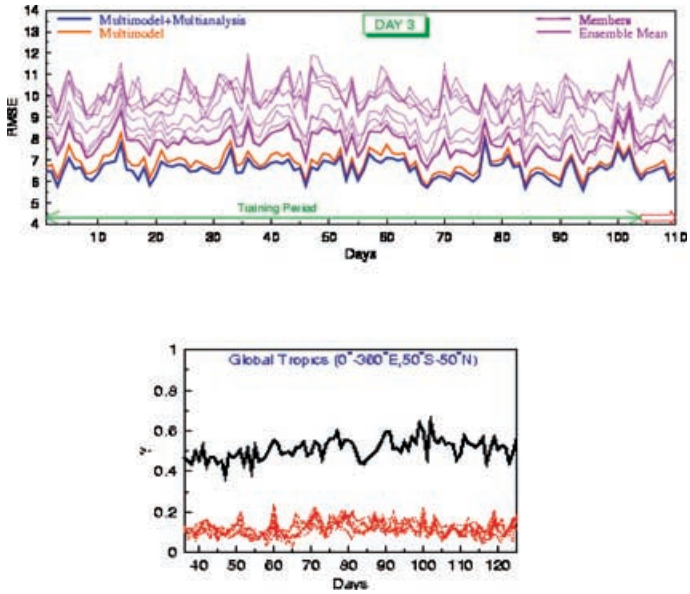

Fig. 2. Day 3 precipitation forecast skill over the global domain during October 2000. (a) RMS errors (mm d^{-1}) for superensemble (based on multimodels and multianalysis), and the results for the individual member models. The color legends are provided within the illustration. (b) Correlation of predicted rain against observed measures (derived from satellite microwave radiances) from member models (red lines) and the superensemble shown by black line.

and the five multianalysis components, a control forecast using FSU global spectral model without physical initialization. These results are relevant to the design of a Unified cumulus parameterization scheme, which is the main objective of this study. We calculate three measures of skill on a regular basis: (i) correlation of model predicted daily rainfall totals and observed estimates; (ii) RMS errors of model predicted daily rainfall totals; (iii) equitable threat scores (Mesinger, 1996) for different thresholds of observed and predicted rain. Figures 2 and 3 illustrate these monthly skills for October 2000. Our results indicate that the multimodel/multianalysis superensemble has a much higher skill when compared to (i) the individual models, (ii) the conventional ensemble mean and (iii) the ensemble mean of the individually bias-removed models. As was summarized in Krishnamurti et al. (2001) the 1- to 3-d forecast skills of the daily precipitation totals for the three metrics used here are indeed highest for the superensemble. The equitable threat scores are also highest for each threshold (0.5–75 mm d^{-1}) for the superensemble. These computations are illustrated on our website (http://lexxy.met.fsu.edu/rtnwp) for many sub-regions of the globe where the results are equally promising. We have also made use of these precipitation forecasts for assessing guidance for the occurrence of local floods. We have thus far examined as many as 10 regional floods arising from heavy rainfall episodes. An example of heavy rains during the passage of Hurricane Allison of the year 2001 over the northern shores of the Gulf of Mexico is illustrated in Fig. 4. The heavy rains and floods affected Texas, Louisiana and the Florida Panhandle during 6–10 June 2001. Even the results for the best model, shown here, did not carry these heavy rains in the region of local floods. There was clearly more skill in the prediction of heavy rains during the passage of Hurricane Allison from the superensemble. The results presented in Figs. 2 and 3 are all for day 3 of forecasts. The day 1 skills were considerably higher (Krishnamurti et al., 2001).

2. Various cumulus parameterization schemes used in the present study

A rather large number of papers have appeared in recent literature on the comparisons of the performance of various cumulus parameterization schemes; Kuo et al. (1996), Wang and Seaman (1997),

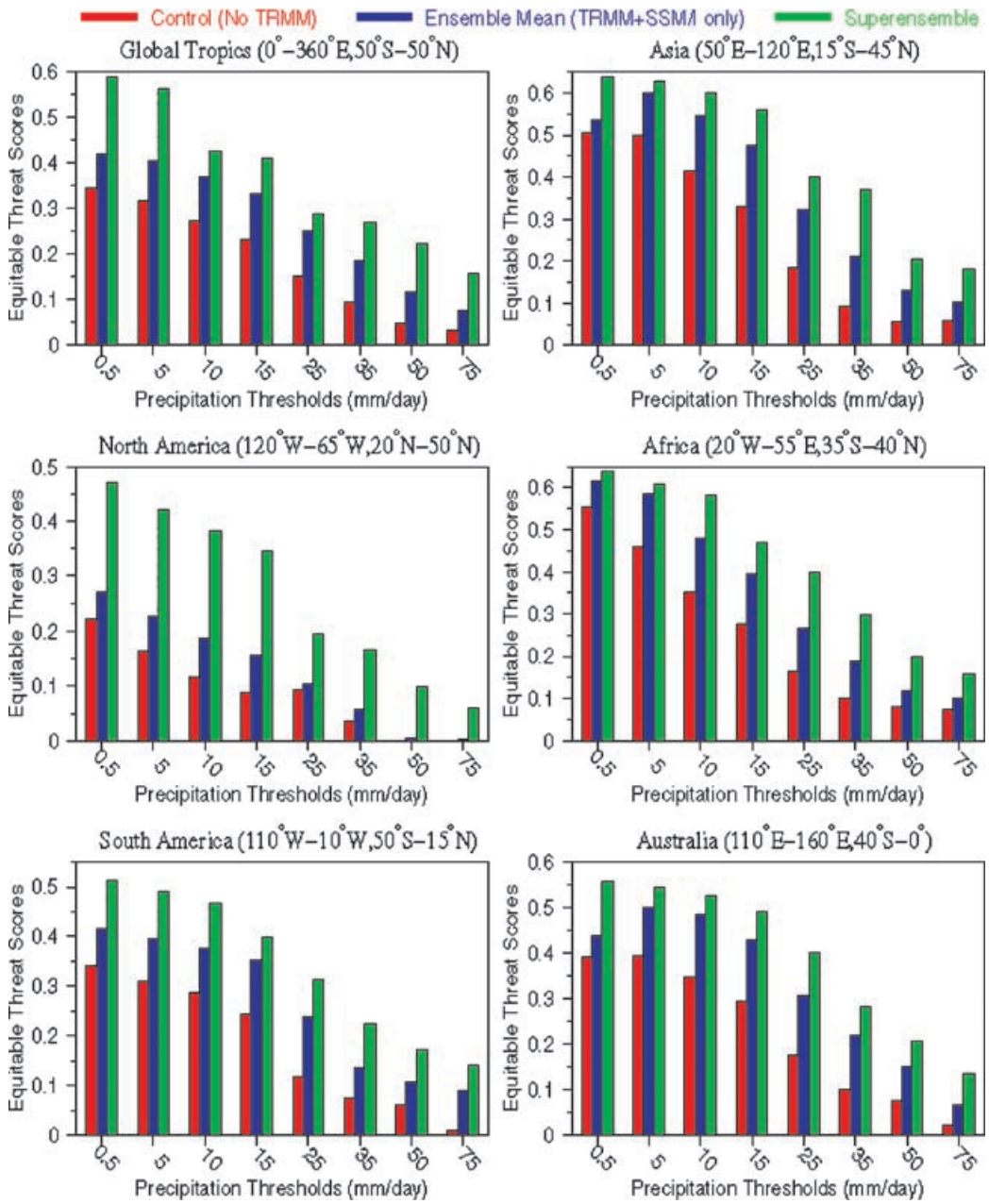

Fig. 3. Equitable threat scores for day 3 precipitation forecasts over different belts for different thresholds of precipitation rates (in mm d^{-1}). Green line shows results for the multimodel multianalysis superensemble. Blue line shows the results for the ensemble mean of the 11 member models and the red line show the results for a member model.

Belair et al. (2000), Ferretti et al. (2000), Rajendran et al. (2002), Das et al. (2001) and several others. The impression one gets from these comparative studies, that are generally based on integrations starting from a few initial states, is that no single cumulus parameterization scheme is superior to another, and that is often a function of the initial state. When we carried out 85 experiments with six different cumulus

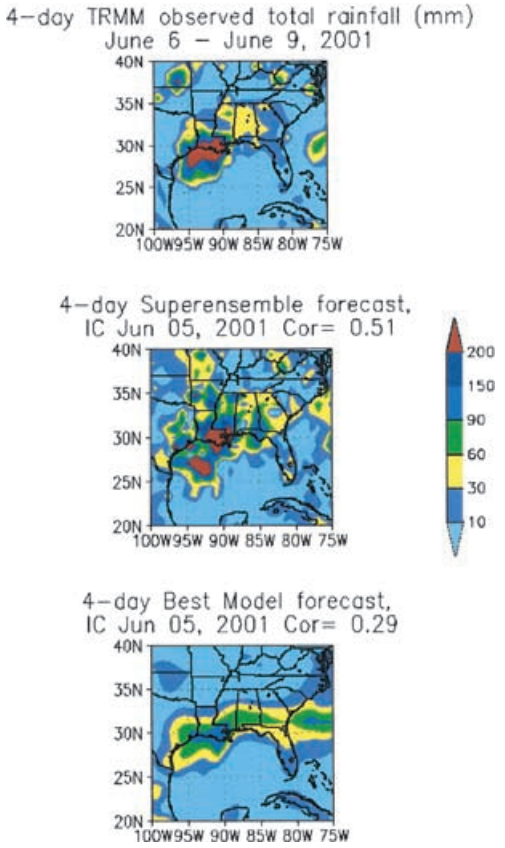

Fig. 4. An example of heavy rain forecast during a flood event covering the passage of hurricane Allison during June 2001. These include the 4 d observations (satellite-based estimates), those from the superensemble forecasts and those from the use of the best model. Units: 4 d totals in mm.

parameterization schemes (Shin and Krishnamurti, 2003a,b) we did see an intersection of their skill score curves (as a function of time). This is depicted in Fig. 5 where we show the precipitation RMS errors and correlations for the six member models (thin lines), the ensemble mean (light, thick line) and the super ensemble (dark, thick line) for day 1 and day 2 forecasts during the training phase over the global belt. This implies that the short-range precipitation forecast skills are often initial value dependent. We shall next describe the various cumulus parameterization schemes used in this study.

2.1. *FSU Modified Kuo Scheme (KUO)*

The basic ingredients of this scheme (Krishnamurti et al., 1980; Krishnamurti and Bedi, 1988) include vertical advection of moisture and differences in temperature and specific humidity between a local moist adiabat and the environmental sounding. Moisture supply for the definition of clouds is given by vertical advection of moisture, whereas difference of temperature and specific humidity define the heating and moistening of a unit vertical column. This scheme furthermore invokes a mesoscale moisture convergence and a moistening parameter which are based on conservation laws for moisture and heat that in turn define the evolving amplitudes for the column heating and moistening. A closure is required for determining these amplitudes, which involves additional large-scale features such as the vertically averaged vertical velocity and the lower tropospheric cyclonic vorticity. This scheme has been tested in numerous studies on tropical weather disturbances by the FSU group, e.g. Krishnamurti et al. (1993, 1994).

2.2. *GSFC Relaxed Arakawa–Schubert Scheme (RAS1)*

This scheme is a simplified form of the Arakawa and Schubert (1974) cumulus parameterization (AS) introduced by Moorthi and Suarez (1992). The complex cloud model in AS is simplified by assuming that the normalized cloud updraft mass flux is a linear function of height and the effects of cloud condensate loading and moisture content in the buoyancy calculations are ignored. The quasi-equilibrium is achieved through relaxation of the sounding towards the equilibrium state in a prescribed time, instead of simultaneously letting all cloud ensembles adjust the environment to a state of equilibrium. This original implementation of RAS is used in the model version using GSFC cumulus code. This version is known to have excessive drying due to the lack of downdraft effects and because of not including the effects of evaporation of falling rain in the environment, which was also a problem with the original AS scheme. In spite of these problems we have used this original RAS version to bring out the diversity in model forecasts when such observed features are not present.

2.3. *NRL-NOGAPS Relaxed Arakawa–Schubert Scheme (RAS2)*

The NOGAPS forecast model uses a variant of the original AS scheme based on a discrete form of the parameterization developed by Lord and Arakawa (1980) and Lord et al. (1982). The closure is simplified by

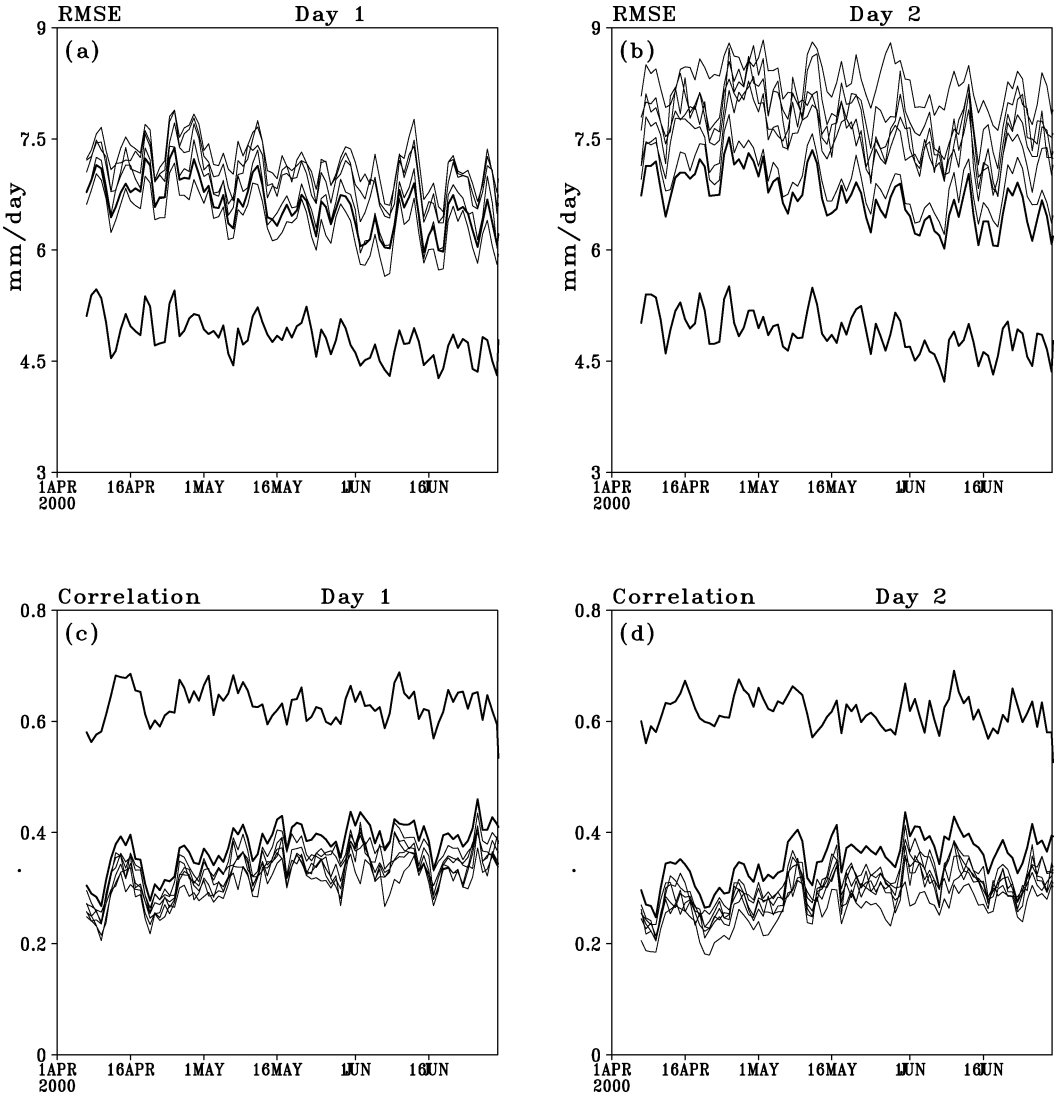

Fig. 5. Precipitation RMS errors (mm d^{-1}) [(a) and (b)], and correlations [(c) and (d)] of member models (thin lines), the ensemble mean (light thick line) and the superensemble forecasts (dark thick line) for day 1 and day 2 over the global belt. These results pertain to the training phase. The results of member models are clustered together in these illustrations, while that for the superensemble with much higher skill stands out.

allowing the environment to be modified through relaxation similar to the RAS scheme by Moorthi and Suarez (1992). In this formulation, the ensemble cloud model is generalized to include the effects of a simple cloud scale moist downdraft. It also includes the low-level moistening effects due to the evaporation of convective precipitation. The moist static energy is conserved during both of these moist processes.

2.4. NCEP Simplified Arakawa–Schubert Scheme (SAS)

In this scheme penetrative convection is simulated following Pan and Wu (1995), which is based on (AS) as simplified by Grell (1993) and with a saturated downdraft. Cloud ensemble is reduced to only one cloud type with detrainment only from its top.

Similar to original AS scheme, it includes the effects of moisture detrainment from convective clouds, warming from environmental subsidence, and convective stabilization in balance with the large-scale destabilization rate. Differing from the general AS formulation, which requires the presence of large-scale atmospheric destabilization with time, SAS uses the rate of change in stability as a major factor to determine convection trigger. It differs from the Grell scheme in the triggering details and the link to large-scale variables. While AS schemes, including Grell, respond to changes in CAPE, the SAS responds instead to differences between model CAPE and a climatological CAPE (from tropical oceans) that varies with cloud height. Over land the scheme allows the atmosphere to completely eliminate CAPE and buoyancy in the presence of large-scale upward vertical motion at the cloud base.

2.5. NCAR Zhang–McFarlane Scheme (ZM)

This simplified cumulus parameterization scheme, developed for climate modeling, was reported in Zhang and McFarlane (1995). This is based on a plume ensemble concept somewhat similar to the original proposition of AS. This scheme addresses penetrative deep convection. This scheme, first tested on a column model, attains equilibrium where large-scale humidity in the tropics in presence of convection is less than the saturation limit. It includes an ensemble of entraining updrafts with an evaporatively driven ensemble of convective scale downdrafts. This scheme is simplified to address the issues of quasi-equilibrium by stating that the same initial mass flux characterizes the cloud base mass flux for updrafts and cloud top mass flux for downdrafts. Furthermore they assume that the fractional entrainment rates are limited to certain values dictated by large-scale thermodynamical structure. In this formulation quasi-equilibrium is accomplished when the production of convective available energy balances the consumption of this quantity by moist convection. Convective available energy is generated by the combined actions of surface fluxes of heat, moisture, radiative cooling and large-scale ascent. The rest of the formulation is quite similar to that of the simplified AS scheme.

2.6. NRL-NOGAPS Emanuel Scheme (ECS)

This cumulus scheme is described in two papers, Emanuel (1991) and Emanuel and Zivkovic-Rothman (1999). Here deep cumulus convection is designed to penetrate the level of neutral buoyancy of the parcel originating as an undiluted sub cloud layer air. Entrained air is what mostly constitutes the mass of these convective clouds. This scheme permits strong saturated downdrafts even in the absence of rain. Stabilization of the boundary layer is accomplished by evaporation of falling rain initiated by the unsaturated downdrafts. An important ingredient of this scheme is the 'buoyancy sorting', a notion introduced by Raymond and Blyth (1986), which assumes that a spectrum of cloud air mixes with different mixing fractions by ascending or descending to the level of vanishing buoyancy. Mixing in clouds is highly intermittent and inhomogeneous in this scheme. Two precipitation formation processes are central in this scheme, i.e. the Bergeron–Findeisen and a stochastic coalescence mechanism. This scheme uses a mass flux parameterization where the flux transports across various sorted levels; this is accomplished by a predictive equation for the mass flux. The roots of convection are assumed to arise from a level where maximum value of the moist static energy is found below the level of an equivalent potential temperature (θ_e) minimum. This permits several possible vertical levels where initiation of convection can occur. Precipitation is generated from prescribed cloud water thresholds for each sample of cloud air. Temperature dependence of this cloud water thresholds account for the definition of ice content. Cloud water and precipitation are essentially separate and do not carry any further interaction. Downdrafts are assumed to have a single predefined cross-section size where heat, water substances and precipitation are transported according to a prescribed rate equation.

We have noted a considerable diversity in the monthly mean performance of the individual models. Although the initial states and the rest of the dynamics and physics of the six member models are the same (except for the aforementioned cumulus parameterizations) the one-day forecasts of rain were quite different. The June 2000 monthly averaged values of rain rates, vertically integrated heat source $\langle Q_1 \rangle$ and moisture sink $\langle Q_2 \rangle$ are illustrated over a North American (Fig. 6) and an Indian monsoon (Fig. 7) domain. The methodology used in the computation of $\langle Q_1 \rangle$ and $\langle Q_2 \rangle$ are discussed in detail in section 4.1. In these figures, the top panel from left to right shows the rain rates from the FSU real time analysis, Krishnamurti et al. (2001), and the estimates of $\langle Q_1 \rangle$ and $\langle Q_2 \rangle$ using the substantial derivatives of the dry static energy

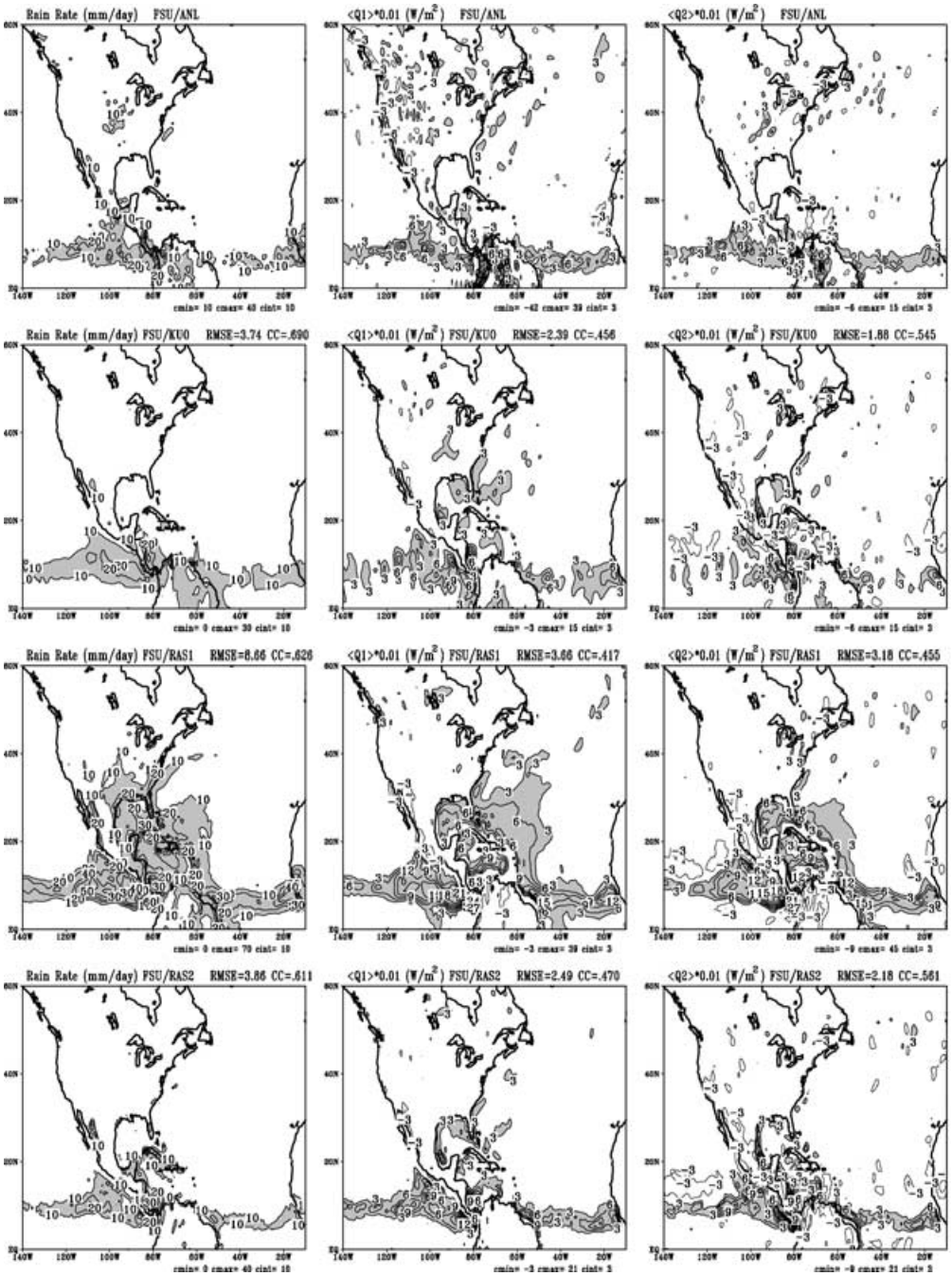

Fig. 6. June 2000 monthly mean vertically integrated apparent heat source $\langle Q_1 \rangle$ and apparent moisture sink $\langle Q_2 \rangle$ based on FSU analysis and the day 1 forecasts from the six member models over the North American region.

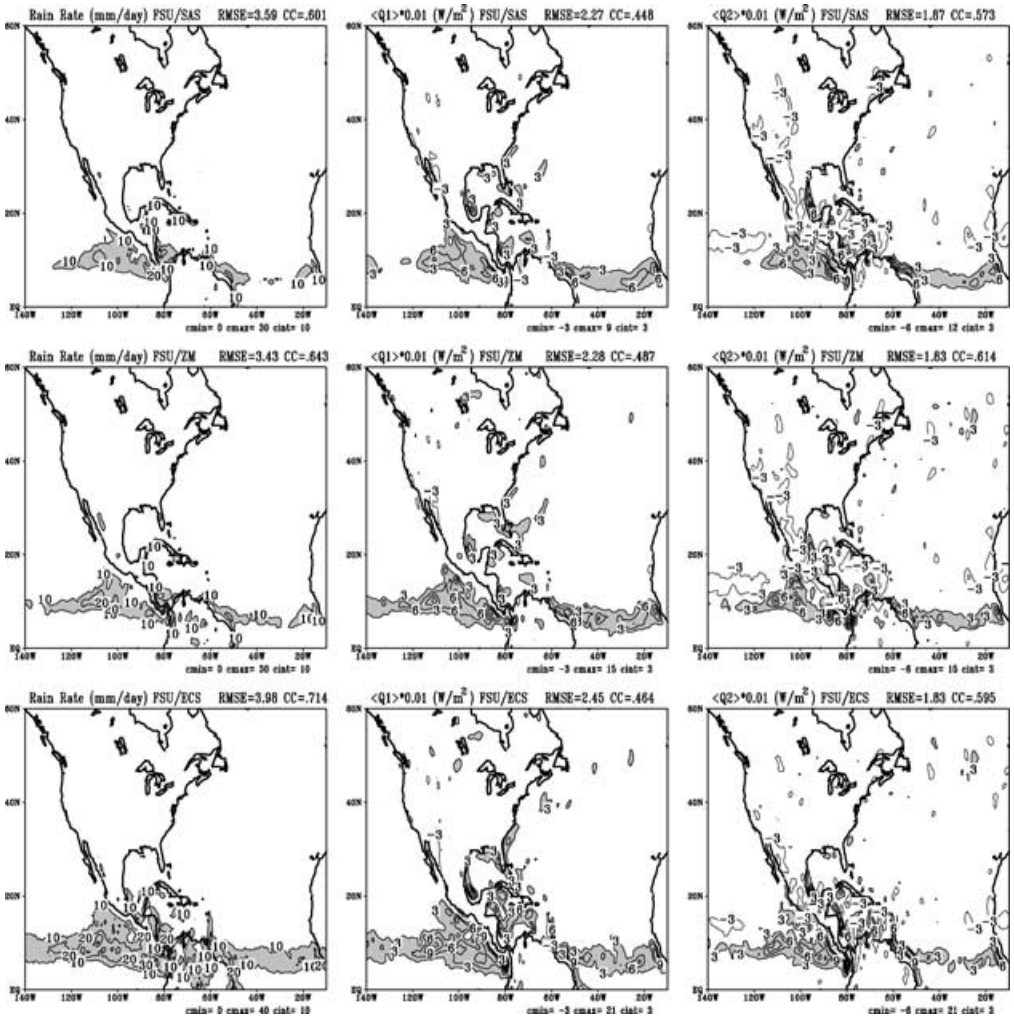

Fig. 6. (cont'd).

and specific humidity based on FSU analysis, which uses ECMWF datasets as first-guess fields. Below that are shown six rows of corresponding forecast results from the use of the six different cumulus parameterization schemes. Here we shall examine the relative performance of the day 1 forecasts of these different schemes averaged over an entire month of June 2000. The performance of the individual schemes can be assessed by visual inspection of the horizontal distribution of the fields. Alternatively one can also look at the spatial correlation and RMS errors of each forecast with respect to the observed estimates. The spread of rainfall over the Arabian Sea and Bay of Bengal (Fig. 7) is somewhat large for RAS1, which does not include downdrafts. This spread is less for SAS. The North American monsoon rainfall (over land areas) is, however, underestimated by SAS and ZM. Overall the performance of most member models for the North American monsoon is deficient. An examination of the RMS errors and the correlation for precipitation forecasts, posted at the top of each forecast panel, shows that for the North American region the spread of correlation range from 0.60 to 0.71, while that for the monsoon rainfall forecasts have a spread of

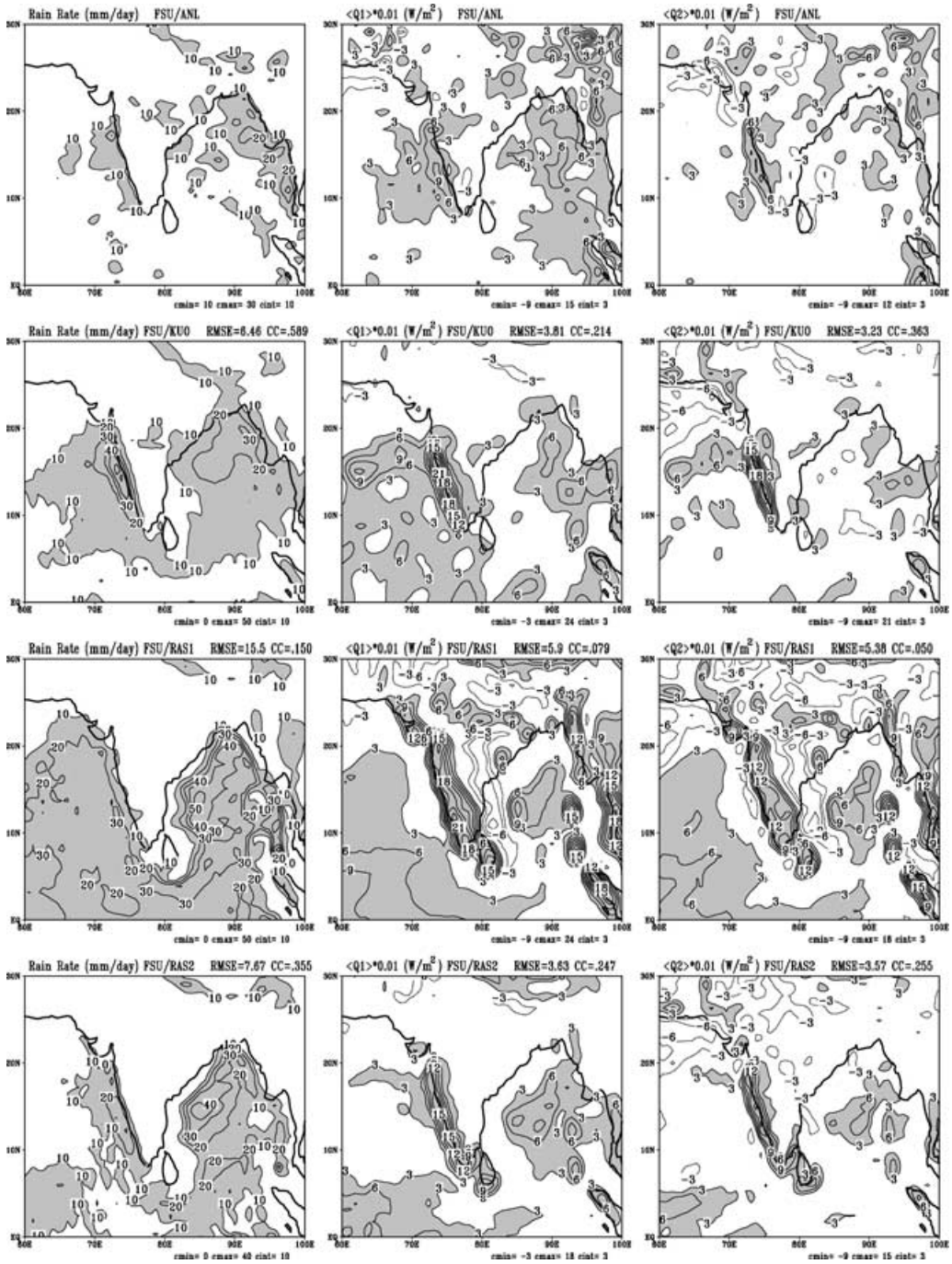

Fig. 7. Same as in Fig. 6, except over the Indian region.

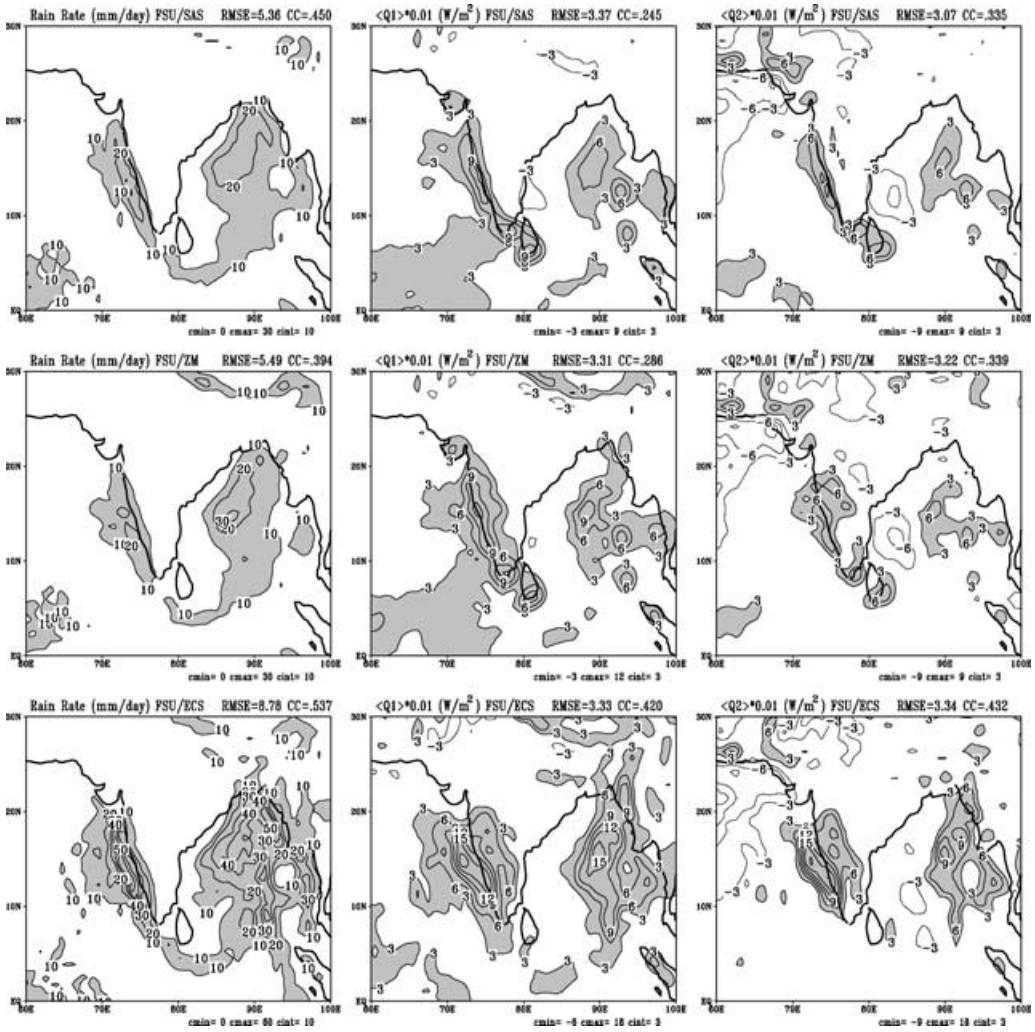

Fig. 7. (cont'd).

correlation between 0.15 and 0.59. Thus the forecasts over the monsoon region appear to show a very large spread. The RMS errors of rainfall over this region also show large spread ranging from 5.36 mm d^{-1} for SAS to 15.5 mm d^{-1} for RAS1 that does not include downdrafts. The range of variability of $\langle Q_1 \rangle$ and $\langle Q_2 \rangle$ are found largest along the ITCZ over the North American belt near 5–10°N. Here the spread of $\langle Q_1 \rangle$ ranges from around 300–600 W m^{-2} for SAS to as high as 1500 W m^{-2} for RAS1 without downdrafts. This range of values is clearly reflected in the respective RMS errors and the correlation. Very similar spreads are also noted for $\langle Q_2 \rangle$ for these same models. Thus it appeared worthwhile to examine a Unified scheme, which has been determined from a larger experimentation program.

3. Distribution of weights and the design of a Unified model

We used 85 d of multimodel day one precipitation forecasts to construct the weights from the training phase. These weights are optimized by selecting those recent 85 d that exhibited highest skills for the precipitation superensemble. For determination of the

weights during the training phase and for the forecast verification (in the forecast phase), observed precipitation estimates are obtained from a continual, once daily, analysis of the precipitation estimates from the TRMM and DMSP satellites.

Global distribution of the statistical weights from training phase of the multimodel superensemble covering a 85-d period prior to 1 July 2000 are illustrated in Fig. 8. The six panels show the weights derived from the precipitation forecasts for six versions of the FSU model that made use of six respective cumulus parameterization schemes. Since the weights vary in space based on their recent past performance skills, in effect there are as many as 131 072 cumulus parameterization schemes over the globe, which is the size of the transform grid (512×256) over the global belt for the model at a resolution T170. The distribution of these weights is monotonically changing, thus over fairly large areas similar weights for a particular cumulus parameterization prevail.

The weights have positive and negative fractional values. Those models that exhibit a better performance during the training phase over a given region carry positive weights and those that performed poorly acquire negative weights. Overall four of the six models appear to carry a large number of points with strong positive weights, whereas two of the models show a spread of negative weights.

We make use of these weights to define the Unified model. This single model utilizes these aforementioned differing weights to incorporate within it the string of six cumulus parameterization schemes to define the respective convective heating rates. These weights are thus obtained by utilizing the large amount of information available from the training phase about the past skill performance (of short-range rainfall forecasts). In these experiments the initial states and the models are identical, except for the cumulus parameterization schemes. It was felt that one day forecast differences that arise in these experiments would thus largely be a function of the varying cumulus parameterization schemes. That is what led us to assign the weights based on day one precipitation forecast skills to the convective heating of the various models.

3.1. When do we invoke convection in the Unified model

When a single cumulus parameterization scheme is used, such as the modified Kuo's scheme (Krishnamurti et al., 1980; Krishnamurti and Bedi, 1988), we had to invoke convection if certain external conditions are met. For the Kuo's scheme it is required that lower tropospheric conditional instability be present at a level along with a large-scale supply of moisture over a unit vertical column. In this instance it is also required that large-scale upward vertical velocity be present at the base of the cloud being invoked. In the Unified model having six different cumulus schemes with differing features (Table 2), the criteria for invoking convection may seem to be complicated. However, since all these schemes are independently strung out within a single model without modifying their individual convection triggering requirements, the implementation becomes relatively easy. Only the end products from these individual cumulus schemes, such as the convective heating and precipitation rates at each model time step, are scaled using the respective superensemble weights, and their cumulative effects modify the model temperature and moisture profiles. This is how presently cumulus convection is invoked in the Unified scheme.

4. Results from multimodel forecasts, the Unified model and the FSU Superensemble

The results from individual multi-model forecasts (during 5 d of the forecast phase) are shown in Figs. 9a–9c for the Global tropics, North American and Asian region. The regional domains are identified on top of these illustrations. Here the results valid on days 1 and 2 of forecasts are shown. The top panels show the RMS errors and the bottom panels show the correlation of the predicted daily rainfall totals with the observed estimates. The vertical barb at the far right (dark, shaded) shows results from the FSU multi-model superensemble, the vertical barb next to it (no shading) shows results from the FSU Unified model that incorporates six cumulus parameterization schemes with varying weights over the global belt. These are the results from the use of 131 072 combinations of the six cumulus parameterization schemes at the model transform grids. The remaining vertical barbs (light, shaded) show the skill scores from individual FSU model members that use one of the same six cumulus parameterization schemes. Overall it is clear from this figure that the FSU superensemble has the least errors. The

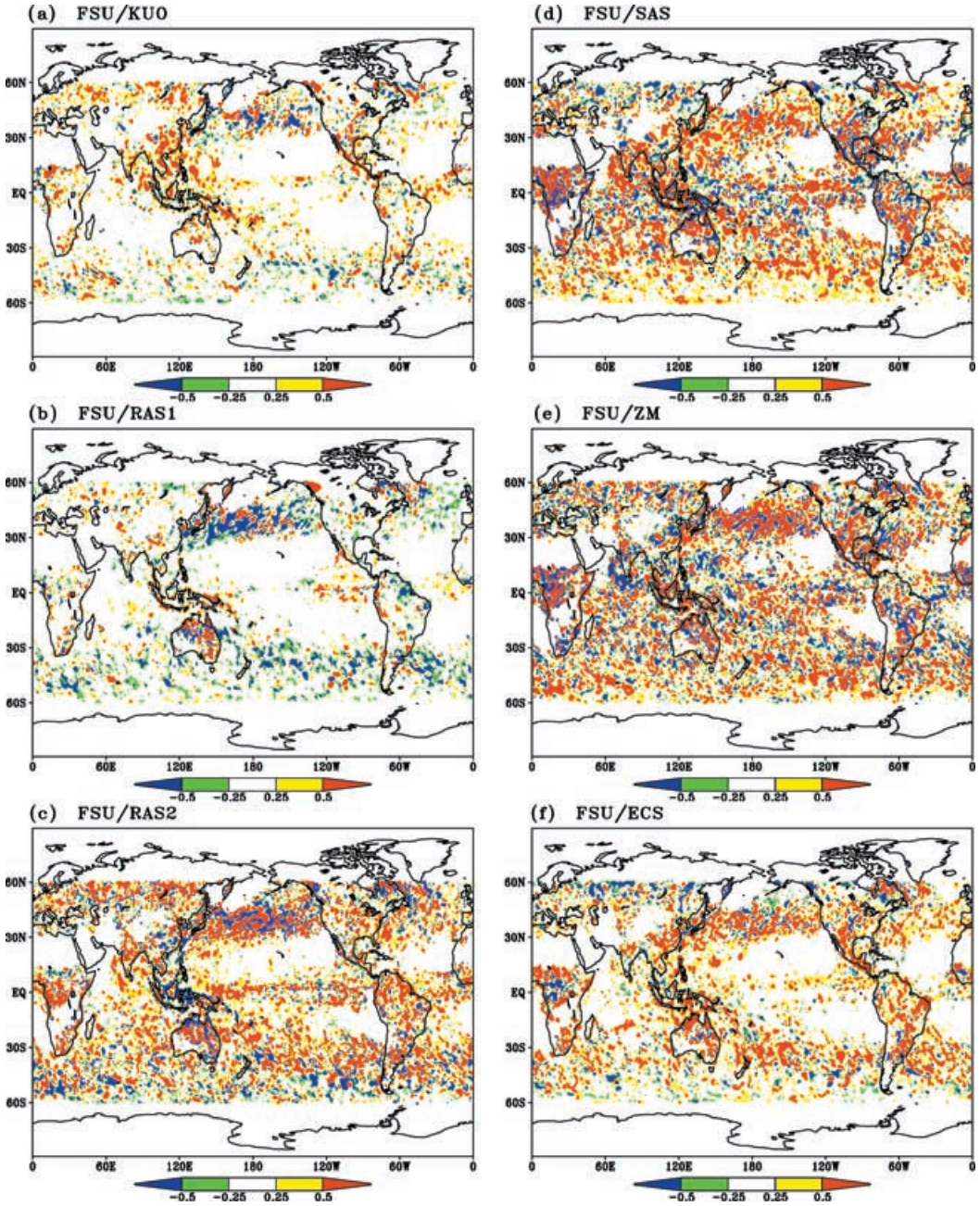

Fig. 8. The global distribution of weights for the six different cumulus parameterization schemes. These are derived from using the same model each time with a separate cumulus parameterization scheme. These weights are determined from the precipitation forecast skills during the training phase of the multimodel superensemble at T170 resolution.

Table 2. *Features among cumulus parameterization schemes*

Sr. No:	Cumulus scheme	Environmental trigger (Modulation of convection by large-scale)	Cloud model (Treatment of cloud thermodynamic properties)	Final state of atmosphere (Quantitative effects of convection on environment)
1.	FSU Modified Kuo	Integrated vertical advection of moisture.	Moist adiabatic lapse rate. No downdrafts.	Tends towards local moist adiabat.
2.	GSFC Relaxed Arakawa-Schubert	Rate of destabilization by advective changes.	Entraining plume model. Invokes single members of a cloud ensemble one after the other. Normalized cloud updraft mass flux linear function of height. No downdrafts.	Relaxes to steady state clouds in prescribed time.
3.	NRL Relaxed Arakawa-Schubert	Rate of destabilization by advective changes.	Includes evaporation of falling rain. With downdrafts.	Relaxes to steady state clouds in prescribed time.
4.	NCEP Simplified Arakawa-Schubert	Rate of change of stability. Upward vertical velocity at cloud base.	Only the deepest cloud considered. Moisture detrainment from convective clouds. Warming from environmental subsidence. Downdrafts and evaporation of falling rain included.	Adjusts toward an equilibrium cloud work function within a specified time.
5.	NCAR Zhang and McFarlene	Plumes of updraft ensemble need to be sufficiently buoyant to penetrate through locally conditional unstable lower troposphere.	Ensemble of entraining updrafts with associated saturated downdrafts.	Removes CAPE at an exponential rate with a specified time. Neutrally buoyant for undiluted reversible ascent of a parcel.
6.	NRL Emanuel	First level of neutral buoyancy for the undiluted, reversible ascent of near surface air is at a higher altitude than level of cloud base.	Sub-cloud scale drafts using buoyancy sorting technique. Determines mass flux prognostically. Stochastic coalescence and Bergeron–Findeisen mechanism. Cloud water in excess of a threshold amount converted to precipitation. Saturated and unsaturated downdrafts.	Adjusts to a local quasi-equilibrium situation, does not depend on the relaxation of cloud work function.

Unified model outperforms all of the single models. The improvements in skill from the FSU superensemble clearly stand out. The Unified scheme appears to be a better way to go than to use a single cumulus parameterization scheme within a single model. The results pertaining to the global tropical belt (Fig. 9a) show that the range of RMS errors for day 1 and day 2 of forecast for the member models are around 10.0 and 12.0 mm d^{-1}, respectively, whereas corresponding figures for the superensemble are around 7.0 and 7.5 mm d^{-1}, respectively. The correlations of the model rain to observed estimates for day 1 and day 2 of forecasts for the member models are around 0.30 and 0.25, respectively, whereas the corresponding figures for the superensemble are around 0.60 and 0.45, respectively. These results pertain to the forecast phase covering the period 29 June to 4 July 2000. The member model's forecast skills for day 1 and day 2 of precipitation are slightly lower than those of the Unified model, whereas the superensemble has significantly higher skill. It is tempting to say that if a very much improved cumulus parameterization scheme were to appear on the scene tomorrow, its use in a single model might receive a ranking of number three in terms of skill scores for precipitation forecasts. The ranking of number two may be held by a Unified model that includes this future 'best scheme' along with the other available schemes in a weighted sense within a single model. The ranking of number one for rainfall forecasts may still be assigned to the multi-model superensemble, which is constructed from a training, and a forecast phase where all available versions of the cumulus parameterization were run separately within single models. Only some 85 separate multimodel experiments have thus far been run, further confirmation of these results could have a significant impact to NWP.

Precipitation forecasts from multimodel superensemble are shown for the global tropical belt in Figs. 10 and 11. This figure includes observed estimates of rain (24 hourly total ending on 1 July 12 UTC and 2 July 12 UTC, respectively, for the year 2000), the predicted rainfall totals from the Unified model, the ensemble mean, the multimodel superensemble and the predicted rainfall from the individual models using the six different single cumulus parameterization schemes. This is a typical example of a tropical precipitation forecast from the models described in this paper. When we look at the different panels of these two illustrations it is difficult to assess a comparison of one panel against another. Some of the prominent heavy rains over southern Bay of Bengal and the western Pacific are noted in the FSU/RAS1, FSU/RAS2, the superensemble and the FSU/KUO panels. It is the overall statistics over a longer period that seems to convey the relative performances better.

4.1. Vertical structure of heating and moistening

For the evaluation of performance of the various cumulus parameterizations we have used precipitation forecast skills as a measure of their reliability. The optimization of the Unified scheme and the FSU superensemble forecast skills addressed above made use of the weights of the precipitation during the pre-forecast training phase. Thus the issue of how well these models carry the vertical profiles of heating and moistening (the apparent heat source, Q_1 and the apparent moisture sink, Q_2, Yanai et al., 1973) was indirect since Q_1 and Q_2 were not optimized for the definition of the proposed weights, those were determined entirely from the past precipitation forecast skills. It is difficult to bring in an optimization of three different parameters R (the rain rates), Q_1 and Q_2. Here Q_1 and Q_2 were calculated, after the fact, in order to assure that the Unified scheme was not running away towards unrealistic values after the forecasts had been completed.

Yanai et al. (1973) definition of Q_1 and Q_2 are as follows:

$$\frac{\partial s}{\partial t} + V \cdot \nabla s + \omega \frac{\partial s}{\partial p} \equiv Q_1 \equiv L(\overline{c} - \overline{e}) - \frac{\partial}{\partial p}\overline{s'\omega'} + Q_R \tag{4}$$

$$-L\left(\frac{\partial q}{\partial t} + V \cdot \nabla q + \omega \frac{\partial q}{\partial p}\right) \equiv Q_2 \equiv L(\overline{c} - \overline{e}) + \frac{\partial}{\partial p}\overline{q'\omega'} \tag{5}$$

where $s = C_p T + gz$ is the dry static energy, T is the temperature, z the height above the ground surface, g the acceleration due to gravity and q the mixing ratio of water vapor. c is the rate of condensation per unit mass of air, e the rate of re-evaporation of cloud and rain water, and the primes denotes the deviation from the average due to unresolved eddies such as cumulus convection and turbulence.

There are two ways for computing the fields of Q_1 and Q_2. One can take model output at adjacent time

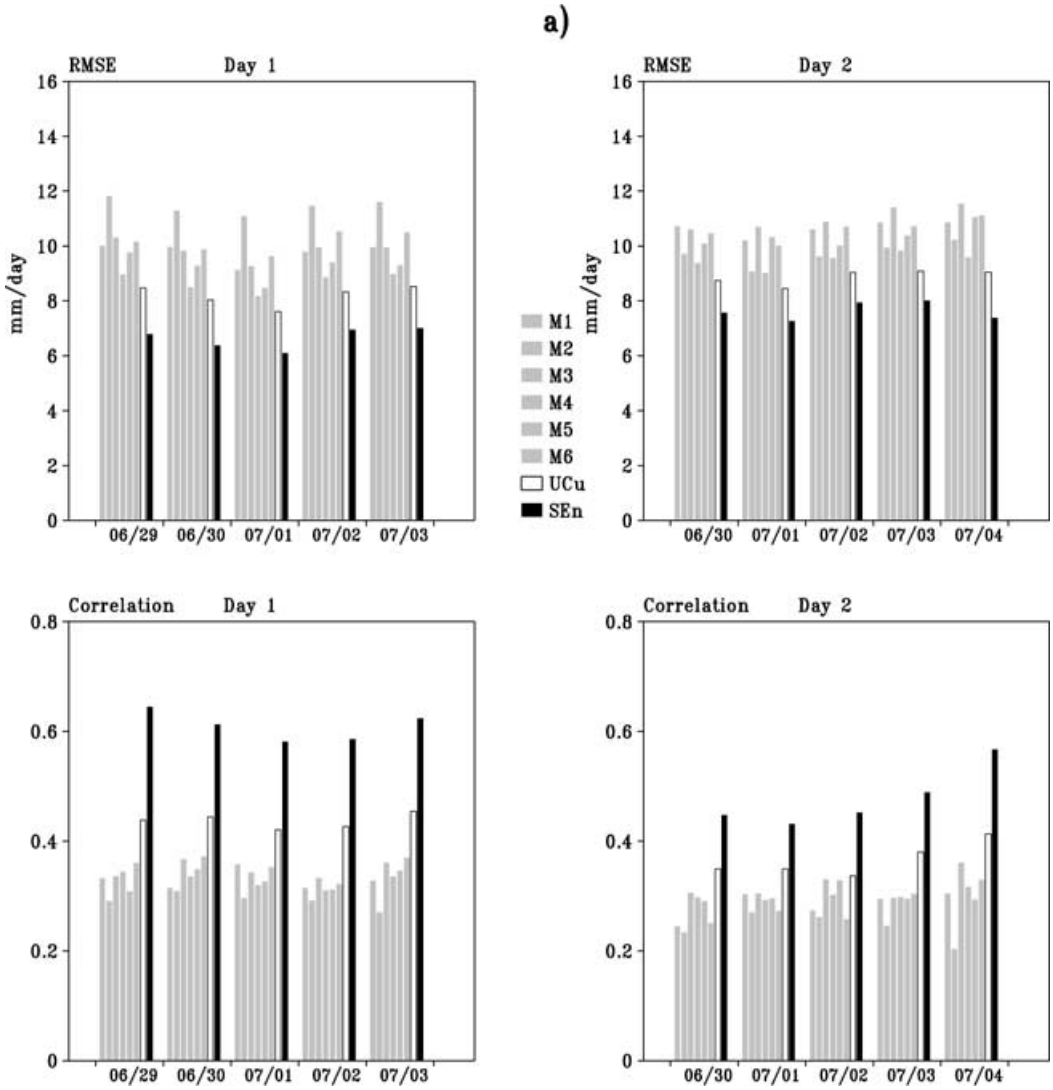

Fig. 9. The results of precipitation forecast skills for the forecast phase of the superensemble for days one and two of forecasts over the (a) Global tropics, (b) North American and (c) Asian regions. The forecasts dates are indicated at the bottom of each panel. The left six vertical barbs in each panel show the performance of the member models, the barb with no shading pertains to the unified model and the black barb that stands out belongs the multimodel superensemble. Units: mm d^{-1}.

steps and calculate the substantial derivatives of the dry static energy s and the (negative of) latent heat $-Lq$. This would provide measures of the left hand side of eqs. (4) and (5). Here computational errors are entirely avoided by using the spectral transform method for the horizontal advective terms and model consistent finite differences for the vertical advective terms. There is, however, a minor difference in the way the model deals with the time differencing (i.e. the semi-implicit scheme) versus what is used here (i.e. central time differencing over a half time step). The second way of estimating Q_1 and Q_2 requires use of the right-hand side of eqs. (4) and (5). The calculation of Q_1 requires the model estimates

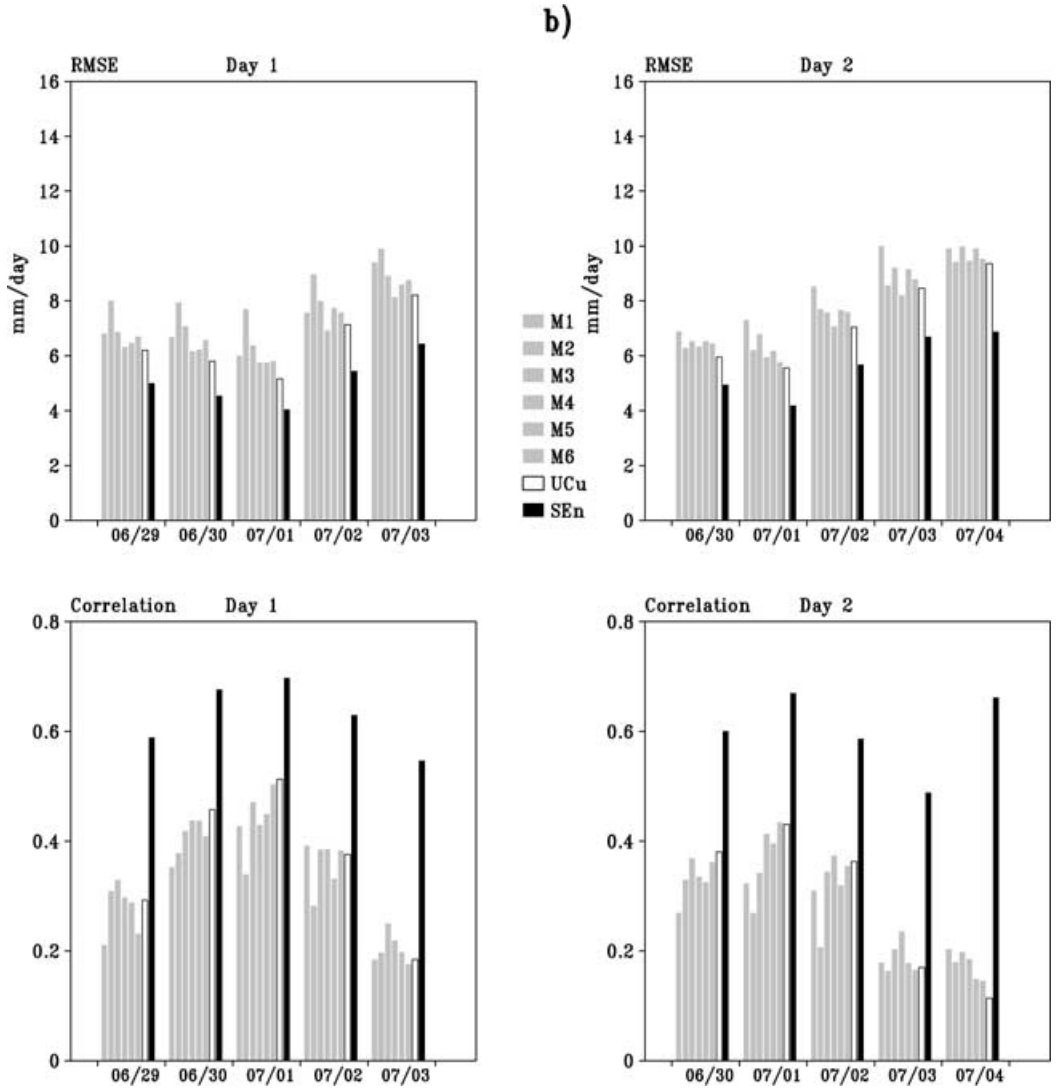

Fig. 9. (cont'd).

of radiation, condensation, evaporation and the eddy convergences of flux of dry static energy. The calculation of Q_2 requires model estimates of condensation, evaporation and the eddy convergence of flux of moisture (in energy units). These equivalent right-hand side terms differ from one cumulus parameterization to another depending on their respective formulations. Given these two possibilities it was easier to present the results for Q_1 and Q_2 based on the left-hand side, i.e. the substantial derivative. However, we did take the trouble to examine the right-hand side as well and confirmed that the two approaches provided nearly equivalent results.

Figure 12 illustrates day 1 forecasts for the (Q_1, Q_2) profiles over a sample convective area. Here vertical distributions for the six individual FSU model members (with single scheme) are shown as thin solid lines; the results for the FSU Unified model (single model containing weighted sum of six cumulus parameterization schemes) are shown as a light dashed

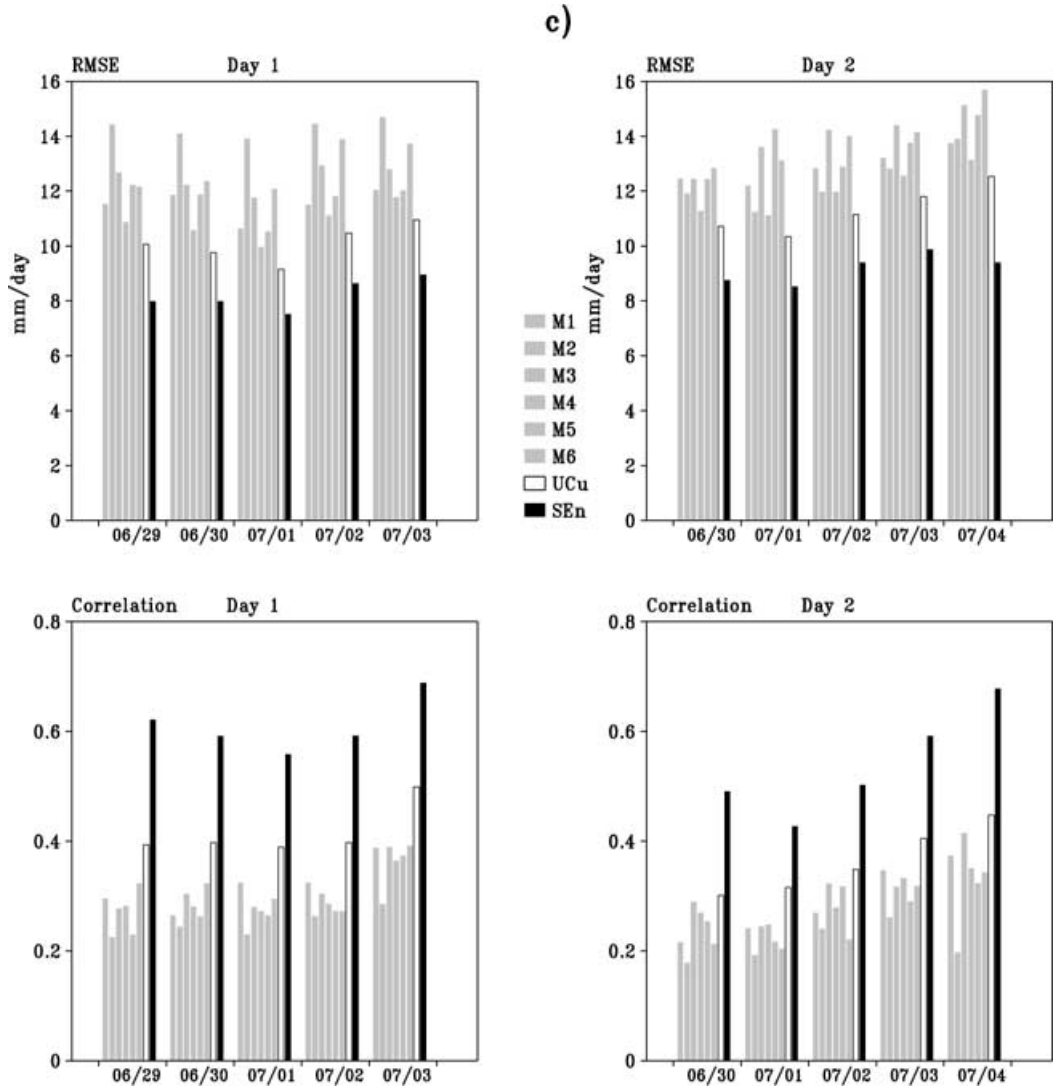

Fig. 9. (cont'd).

line, the ensemble mean as a dark dashed line, the FSU multimodel superensemble results as a light solid line and the observed estimates are shown as a dark solid line. The observed estimates came from the analysis data sets of ECMWF. Here 24 hourly analyses were available, hence the time tendencies of the static energy and specific humidity were based on those time intervals. The advective terms, horizontal and vertical, were determined from the use of spectral transform method and finite differences, respectively. Construction of vertical profiles for the multimodel superensemble involved optimization of the Q_1 and Q_2 weights at each model sigma levels from 85 experiments with the six individual model members during the training phase. It is clear from this diagram that the best results arise from the multimodel superensemble, the member models show a considerable spread and the Unified model appears to carry these profiles reasonably well compared to the observations.

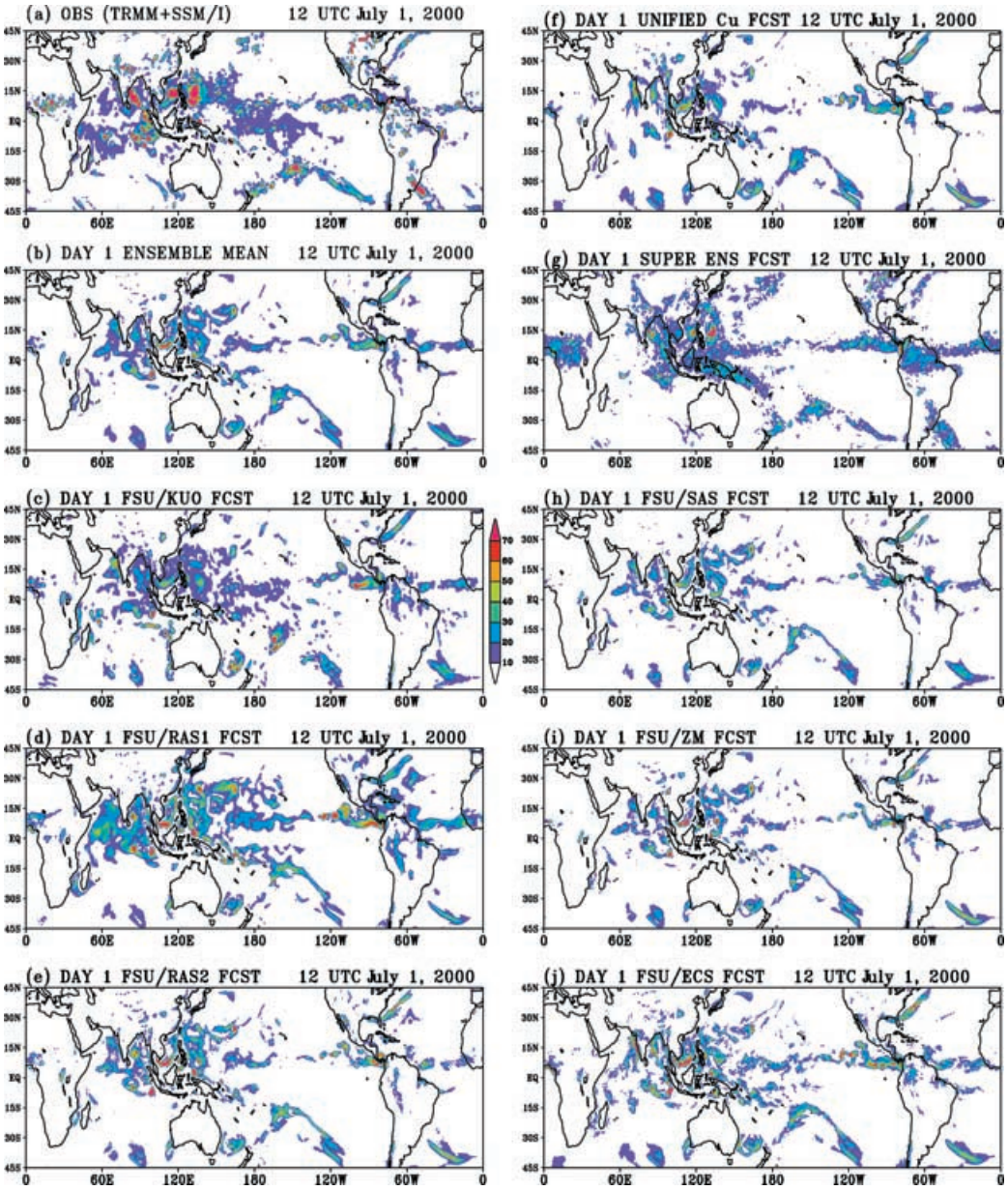

Fig. 10. A sample of observed rainfall estimates and those produced from model forecasts for day 1 of forecasts from the following: Unified model, ensemble mean of model forecasts, multimodel superensemble and from six member models. Units: mm d^{-1}.

5. Summary and conclusions

Table 2 lists various physically based cumulus parameterization schemes that invoke a number of processes such as detrainment, massflux, moisture convergence, plume ensemble model, restoration of moist static instability, saturated and unsaturated downdrafts, buoyancy sorting, conversion of cloud and ice water, etc. The proposed Unified scheme is physically based since it does include all of these processes.

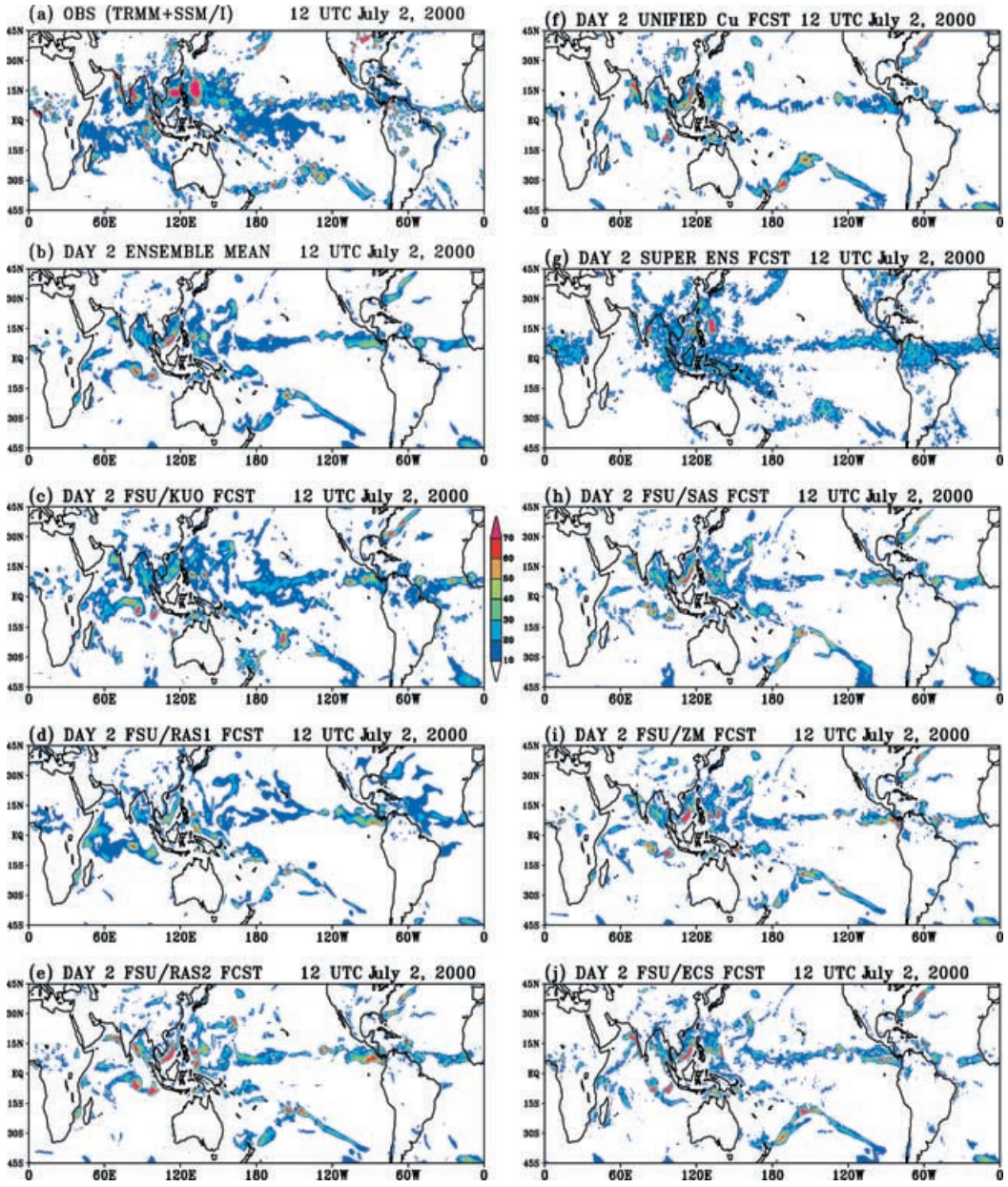

Fig. 11. Same as in Fig. 10, but for day 2 of forecasts.

There are in fact 131 072 cumulus parameterization schemes that were deployed over the global domain in this study. The superensemble methodology, which was needed to determine these globally distributed weights, is an important component of this study. Although, that many weighted combination of the six basic schemes may not have been necessary, it was felt that coding that degree of regional variability was a relatively simple matter. The rationale here is that a parameter such as moisture convergence provides a good measure of rain over some regions, such as the Eastern Atlantic (Reed et al., 1977), it is not the best

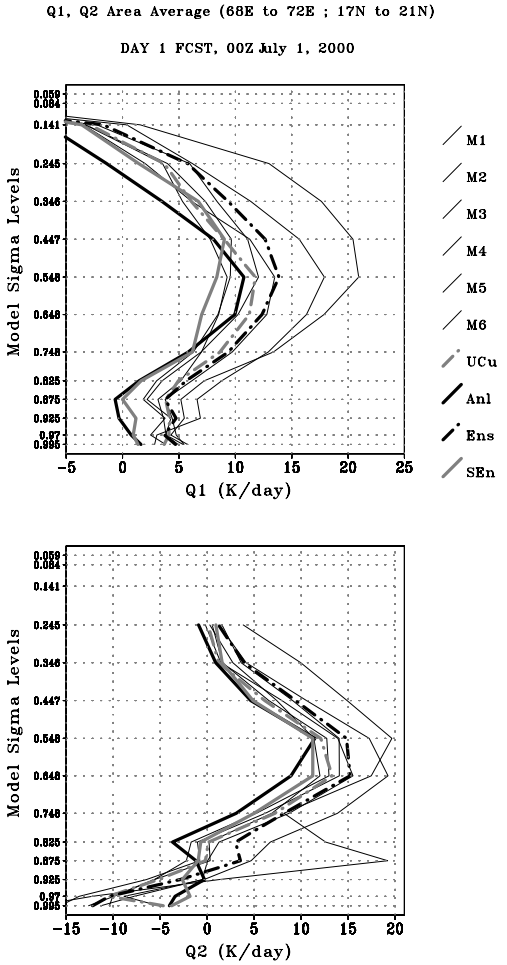

Fig. 12. Vertical profiles of the apparent heat source, Q_1, and the apparent moisture sink, Q_2, units: K d^{-1}. Thin solid lines show the results for the member models. The light dashed line shows the results from the Unified model (UCu), the dark solid line pertains to the observed measures (Anl), the ensemble mean (Ens) is represented by the dark dashed line and the results for the multimodel superensemble (SEn) are shown by the light solid line.

measure of deep convection at some other places. Likewise, we perceive that no single mechanism, illustrated in Table 2, is the best measure for deep convective processes globally. Just as data uncertainties call for a host of initial perturbations in ensemble forecasts (Toth and Kalnay, 1993; Palmer and Tibaldi, 1988), likewise we feel that the current parameterizations of physical processes carry a high degree of uncertainty. A Unified ensemble approach can provide benefits especially if they are cast in the spirit of the superensemble, where the weights determined for their individual past performance could be extended to develop a Unified physical parameterization. While carrying out these forecasts with individual models, we have deliberately limited the forecasts to one or at most two days, towards the design of this Unified scheme. The models used here are all identical except for the cumulus parameterization schemes and furthermore all of these models used the same set of initial states. Thus, we have tacitly assumed that very short-term differences in rainfall forecasts arise from the differences in their respective cumulus parameterizations.

Further improvements from the Unified model are possible if we construct the superensemble by optimizing Q_1 and Q_2 at each vertical level. Currently we have only used the past precipitation forecasts to construct and assign statistical weights for convective heating. If the weights were directly determined for Q_1 and Q_2 in addition to using the rain rates, the performance of the Unified model could have been improved even further.

In the current NWP practice one notes only miniscule improvements arising in the forecast skills from the refinements of physical parameterizations. An example of such was noted by John (2001), where the replacement of a radiative transfer code from a former emissivity/absorptivity algorithm to an explicit cloud-resolving algorithm only yielded an improvement in the anomaly correlation of roughly 1/5 of a percent. The notable improvements from the ensemble mean and the superensemble, illustrated here, demonstrates an order-of-magnitude higher improvement of skill. The future improvements in NWP appear painstaking but are necessary.

In closing, we illustrate an example, Fig. 13, on the reduction of systematic error from an entire year of multimodels and superensemble forecasts. It is clear that the superensemble drastically reduces large systematic errors found in the models with the highest and lowest skills and in the ensemble mean. It is this feature that makes performance of the superensemble considerably higher than the individual models or even the Unified model. The Unified model appears somewhat appealing, and one can in principle construct such Unified models for specific physical parameterizations such as the planetary boundary layer and radiative transfer. Thus collectively it may be possible to improve the performance considerably further from the design of a grand Unified model. In spite of those possible improvements we recognize that if the Unified model is improved within one single model it may still not be able to compete with a multimodel

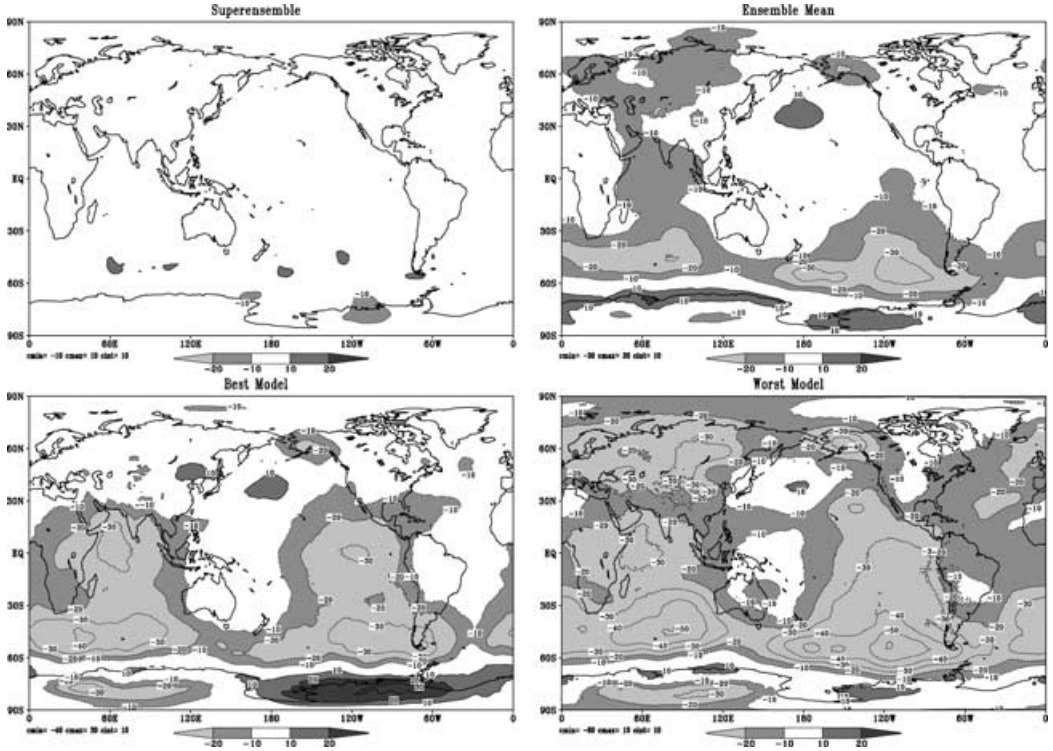

Fig. 13. Day 2 forecast systematic errors of 500 hPa geopotential heights (m) over the global domain during the entire year 2000 (Ross and Krishnamurti, 2003). This includes the mean forecast errors for superensemble (based on multimodels and multianalysis), the ensemble mean and the results for the best and the worst of the 11 member models.

superensemble. The latter can provide a diversity from the global modeling community, which always seems to produce superior forecasts.

6. Acknowledgements

This work could not have been completed without the datasets provided by the following global weather centers: ECMWF, NCEP, NRL, BMRC, RPN and JMA. The precipitation estimates were derived from the microwave radiances provided by TRMM and DMSP satellites. This work was supported by the following grants: NSF ATM-0108741, NASA TRMM NAG5-9662, NOAA NA06GP0512 and NOAA NA16GP1365.

7. Appendix: an outline of the FSU global spectral model

The global model used in this study is identical in all respects to that used in Krishnamurti et al. (1991). The T170 version of the model, however, has been highly vectorized to reduce the model integration time. In addition, moisture variable, dew point depression ($T-T_d$) has been replaced by specific humidity and a look-up table is used for calculating saturation vapor pressure to further reduce the computational time. An outline of the model is as follows:

(1) Independent variables: longitude (λ), latitude (ϕ), vertical coordinate (σ) and model time step (t).

(2) Dependent variables: vorticity, divergence, temperature and specific humidity. Horizontal resolution: Triangular spectral truncation; T170 resolution has a 512×256 Gaussian transform grid with a horizontal separation of about 80 km at 20° latitude.

(3) Vertical resolution: 14 layers in the vertical between 50 hPa and 1000 hPa. Model variables are staggered in the vertical using Charney–Phillips vertical discretization: vorticity, divergence, wind and geopotential are located at layer interface while temperatures, specific humidity and vertical velocity are

assigned at the center of the layer. The vertical grid has higher resolution in stratosphere (two model layers) and in planetary boundary layer (three model layers).

(4) Time integration scheme: The divergence equation, thermodynamic equation and pressure tendency equation are integrated implicitly while for vorticity equation and moisture continuity equation explicit time integration scheme is used. The tendencies of the physical processes are integrated using a forward time integration scheme.

(5) Space differing scheme: Spectral in the horizontal; centered differences in the vertical for all variables except moisture which is handled by an upstream differencing scheme.

(6) Surface topography is based on envelope orography (Wallace et al., 1983).

(7) Parameterization of physical processes: (a) Deep convection: based on modified Kuo cumulus parameterization scheme (Krishnamurti et al., 1983), where the moistening and mesoscale convergence parameters are obtained from 700 mb vorticity and mean vertical velocity averaged over cloud depth through a regression relation. (b) Shallow convection (Tiedke, 1984). (c) Dry convection. (d) Large-scale condensation (Kanamitsu, 1975). The scheme accounts for evaporation of falling precipitation. (e) Surface fluxes of heat, moisture and momentum are calculated using similarity theory (Businger et al., 1971). (f) Vertical distribution of fluxes in the free atmosphere is based on stability (Richardson number) dependent exchange coefficient (Louis, 1979). (g) fourth -order horizontal diffusion (Kanamitsu et al., 1983). (h) Long- and short-wave radiative fluxes are based on band model and incorporate the radiative effects of water vapor, carbon dioxide, ozone and clouds (Harshvardan and Corsetti, 1984; Lacis and Hansen, 1974). (i) Parameterization of low, medium and high clouds for radiative transfer calculation is based on threshold relative humidity. Fractional area of various cloud distribution configurations in the vertical is based on random overlap consideration. (j) Surface temperatures: Prescribed over the oceans, while over the land a surface energy balance coupled to the similarity theory determines the surface temperature including its diurnal cycle (Krishnamurti et al., 1991).

(8) Nonlinear normal mode initialization: (Kitade, 1983), wherein the tendencies of the first five modes with phase speed exceeding about 30 m s^{-1} are damped during the initialization. The slow moving higher modes are allowed to adjust freely.

REFERENCES

Arakawa, A. and Schubert, W. H. 1974. Interaction of a cumulus cloud ensemble with the large-scale environment, Part I. *J. Atmos. Sci.* **31**, 674–701.

Bélair, S., Méthot, M. A., Mailhot, J., Bilodeau, B., Patoine, A., Pellerin, G. and Côté, J. 2000. Operational Implementation of the Fritsch–Chappell Convective Scheme in the 24-km Canadian Regional Model. *Wea. Forecasting* **15**, 257–275.

Businger, J. A., Wyngard, J. C., Izumi, Y. and Bradley, E. F. 1971. Flux profile relationship in the atmospheric surface layer. *J. Atmos. Sci.* **28**, 181–189.

Das, S., Mitra, A. K., Iyengar, G. R. and Mohandas, S. 2001. Comprehensive test of different cumulus parameterization schemes for the simulation of the Indian summer monsoon. *Meteorol. Atmos. Phys.* **78**, 227–244.

Emanuel, K. A. 1991. A scheme for representing cumulus convection in large-scale models. *J. Atmos. Sci.* **48**, 2313–2335.

Emanuel, K. A. and Zivkovic-Rothman, M. 1999. Development and evaluation of a convection scheme for use in climate models. *J. Atmos. Sci.* **56**, 1766–1782.

Ferretti, R., Paolucci, T., Zheng, W., Guido Visconti, and Bonelli, P. 2000. Analyses of the precipitation pattern on the Alpine region using different cumulus convection parameterizations. *J. Appl. Meteorol.* **39**, 182–200.

Grell, G. A. 1993. Prognostic evaluation of assumptions used by cumulus parameterizations. *Mon. Wea. Rev.* **121**, 764–787.

Harshvardan and Corsetti, T. G. 1984. *Long-wave parameterization for the UCLA/GLAS GCM*. NASA Tech. Memo. 86072, Goddard Space Flight Center, Greenbelt, MD, 52 pp.

John, P. G. 2001. Implementation of a shortwave radiation parameterization scheme in the NCMRWF operational global model. In: *Research activities in atmospheric and oceanic modelling*. Rep. No: 31, WMO/TD No. 1064, 4.3–4.4.

Kanamitsu, M. 1975. On numerical prediction over a global tropical belt. Dept. of Meteorology Rep. 75-1, Florida State University, Tallahassee, FL, 282 pp.

Kanamitsu, M., Tada, K., Kudo, K., Sato, N. and Ita, S. 1983. Description of the JMA operational spectral model. *J. Meteorol. Soc. Jpn*. **61**, 812–828.

Kitade, T. 1983. Nonlinear normal mode initialization with physics. *Mon. Wea. Rev.* **111**, 2194–2213.

Krishnamurti, T. N. and Bedi, H. S. 1988. Cumulus parameterization and rainfall rates III. *Mon. Wea. Rev.* **116**, 583–599.

Krishnamurti, T. N., Ramanathan, Y., Pan, H. L., Pasch, R. J. and Molinari, J. 1980. Cumulus parameterization and rainfall rates I. *Mon. Wea. Rev.* **108**, 465–472.

Krishnamurti, T. N., Low-Nam, S. and Pasch, R. 1983. Cumulus parameterization and rainfall rates II. *Mon. Wea. Rev.* **111**, 815–828.

Krishnamurti, T. N., Xue, J., Bedi, H. S., Ingles, K. and Oosterhof, D. 1991. Physical initialization for numerical weather prediction over the tropics. *Tellus* **43AB**, 53–81.

Krishnamurti, T. N., Bedi, H. S. and Ingles, K. 1993. Physical initialization using SSM/I rain rates. *Tellus* **45A**, 247–269.

Krishnamurti, T. N., Bedi, H. S., Oosterhof, D. and Hardiker, V. 1994. The formation of hurricane Frederic of 1979. *Mon. Wea. Rev.* **122**, 1050–1074.

Krishnamurti, T. N., Kishtawal, C. M., LaRow, T., Bachiochi, D., Zhang, Z., Williford, C. E., Gadgil, S. and Surendran, S. 1999. Improved weather and seasonal climate forecasts from multimodel superensemble. *Science* **285**, 1548–1550.

Krishnamurti, T. N., Kishtawal, C. M., Zhang, Z., LaRow, T., Bachiochi, D., Williford, C. E., Gadgil, S. and Surendran, S. 2000a. Multimodel ensemble forecasts for weather and seasonal climate. *J. Climate* **13**, 4196–4216.

Krishnamurti, T. N., Kishtawal, C. M., Shin, D. W. and Williford, C. E. 2000b. Improving tropical precipitation forecasts from a multianalysis superensemble. *J. Climate* **13**, 4217–4227.

Krishnamurti, T. N., Surendran, S., Shin, D. W., Correa-Torres, R. J., Vijayakumar, T. S. V., Williford, C. E., Kummerow, C., Adler, R. F., Simpson, J., Kakar, R., Olson, W. S. and Turk, F. J. 2001. Real-time multianalysis-multimodel superensemble forecasts of precipitation using TRMM and SSM/I products. *Mon. Wea. Rev.* **129**, 2861–2883.

Krishnamurti, T. N., Stefanova, L., Chakraborty, A., Vijayakumar, T. S. V., Cocke, S., Bachiochi, D. and Mackey, B. 2002. Seasonal forecasts of precipitation anomalies for North American and Asian monsoons. *J. Meteorol. Soc. Jpn*., in press.

Kuo, Y.-H., Reed, R. J. and Liu, Y.-B. 1996. The ERICA IOP 5 storm. Part III: Mesoscale cyclogenesis and precipitation parameterization. *Mon. Wea. Rev.* **124**, 1409–1434.

Lacis, A. A. and Hansen, J. E. 1974. A parameterization for the absorption of solar radiation in the earth's atmosphere. *J. Atmos. Sci.* **31**, 118–133.

Lord, S. J. and Arakawa, A. 1980. Interaction of a cloud ensemble with the large-scale environment. Part II. *J. Atmos. Sci.* **37**, 2677–2692.

Lord, S. J., Chao, W. C. and Arakawa, A. 1982. Interaction of a cumulus cloud ensemble with the large-scale environment. Part IV: The discrete model. *J. Atmos. Sci.* **39**, 104–113.

Louis, J. F. 1979. A parametric model of vertical eddy fluxes in the atmosphere. *Boundary-Layer Meteorol.* **17**, 187–202.

Mesinger, F. 1996. Improvements in quantitative precipitation forecasts with the Eta regional model at the NCEP: The 48-km upgrade. *Bull. Am. Meteorol. Soc.* **77**, 2637–2649.

Moorthi, S. and Suarez, M. J. 1992. Relaxed Arakawa–Schubert: A parameterization of moist convection for general circulation models. *Mon. Wea. Rev.* **120**, 978–1002.

Palmer, T. N. and Tibaldi, S. 1988. On the prediction of forecast skill. *Mon. Wea. Rev.* **116**, 2453–2480.

Pan, H.-L. and Wu, W.-S. 1995. *Implementing a mass flux convection parameterization package for the NMC medium-range forecast model. NMC Office Note*, No. 409, 40 pp. [Available from NCEP, 5200 Auth Road, Washington, DC 20233].

Rajendran, K., Nanjundiah, R. S. and Srinivasan, J. 2002. Comparison of seasonal and intraseasonal variation of tropical climate in NCAR CCM2 GCM with two different cumulus schemes. *Meteorol. Atmos. Phys.* **79**, 57–86.

Raymond, D. J. and Blyth, A. M. 1986. A stochastic mixing model for nonprecipitating cumulus clouds. *J. Atmos. Sci.* **43**, 2708–2718.

Reed, R. J., Norquist, D. C. and Recker, E. E. 1977. The structure and properties of African wave disturbances as observed during phase III of GATE. *Mon. Wea. Rev*, **105**, 317–333.

Ross, R. S. and Krishnamurti, T. N. 2003. Reduction of systematic errors for global numerical weather prediction from the FSU superensemble. *Meteorol. Atmos. Phys.*, in press.

Shin, D. W. and Krishnamurti, T. N. 2003. Short- to medium-range superensemble precipitation forecasts using satellite products. Part I: Deterministic forecasting. *J. Geophys. Res.*, **108**(D8), 10.1029/2001JD001510, in press.

Shin, D. W. and Krishnamurti, T. N. 2003. Short- to medium-range superensemble precipitation forecasts using satellite products. Part II: Probabilistic forecasting. *J. Geophys. Res.*, **108**(D8), 10.1019/2001JD001511, in press.

Tiedke, M. 1984. *The sensitivity of the time-mean large-scale flow to cumulus convection in the ECMWF model.* Proc., Workshop on Convection in Large-scale Numerical Models. ECMWF, Reading, U.K., 297–316.

Toth, Z. and Kalnay, E. 1993. Ensemble forecasting at NMC: The generation of perturbations. *Bull. Am. Meteorol. Soc.* **74**, 2317–2330.

Wallace, J. M., Tibaldi, S. and Simmons, A. J. 1983. Reduction of systematic forecast errors in the ECMWF model through the introduction of envelope orography. *Quart. J. R. Meteorol. Soc.* **109**, 683–718.

Wang, W. and Seaman, N. L. 1997. A comparison study of convective parameterization schemes in a mesoscale model. *Mon. Wea. Rev.* **125**, 252–278.

Yanai, M., Esbensen, S. and Chu, J. H. 1973. Determination of bulk properties of tropical cloud clusters from large-scale heat and moisture budgets. *J. Atmos. Sci.* **30**, 611–627.

Zhang, G. J. and McFarlane, N. A. 1995. Sensitivity of climate simulations to the parameterization of cumulus convection in the Canadian Climate Centre general circulation model. *Atmos.-Ocean.* **33**, 407–446.